



Published in final edited form as:

*Nat Neurosci.* 2016 November ; 19(11): 1513–1522. doi:10.1038/nn.4380.

## ***Foxp2* Controls Synaptic Wiring of Corticostriatal Circuits and Vocal Communication by Opposing *Mef2C***

Yi-Chuan Chen<sup>1,7</sup>, Hsiao-Ying Kuo<sup>1,7</sup>, Ulrich Bornschein<sup>2</sup>, Hiroshi Takahashi<sup>3</sup>, Shih-Yun Chen<sup>1</sup>, Kuan-Ming Lu<sup>1</sup>, Hao-Yu Yang<sup>1</sup>, Gui-May Chen<sup>1</sup>, Jing-Ruei Lin<sup>1</sup>, Yi-Hsin Lee<sup>1</sup>, Yun-Chia Chou<sup>1</sup>, Sin-Jhong Cheng<sup>4</sup>, Cheng-Ting Chien<sup>4</sup>, Wolfgang Enard<sup>5</sup>, Wulf Hevers<sup>2</sup>, Svante Pääbo<sup>2</sup>, Ann M. Graybiel<sup>6,\*</sup>, and Fu-Chin Liu<sup>1,\*</sup>

<sup>1</sup>Institute of Neuroscience, National Yang-Ming University, Taipei 11221, Taiwan

<sup>2</sup>Department of Evolutionary Genetics, Max Planck Institute for Evolutionary Anthropology, Leipzig 04103, Germany

<sup>3</sup>Department of Neurology, National Hospital Organization, Tottori Medical Center, Tottori 689-0203, Japan

<sup>4</sup>Neuroscience Program in Academia Sinica, Institute of Molecular Biology, Academia Sinica, Taipei 11529, Taiwan

<sup>5</sup>Anthropology and Human Genomics, Department Biology II, Ludwig-Maximilians University, Munich 82152, Germany

<sup>6</sup>McGovern Institute for Brain Research and Department of Brain and Cognitive Sciences, Massachusetts Institute of Technology, Cambridge, MA 02139, USA

### **Abstract**

Cortico-basal ganglia circuits are critical for speech and language and are implicated in autism spectrum disorder (ASD), in which language function can be severely affected. We demonstrate that in the striatum, the gene, *Foxp2*, negatively interacts with the synapse suppressor, *Mef2C*. We present causal evidence that *Mef2C* inhibition by *Foxp2* in neonatal mouse striatum controls synaptogenesis of corticostriatal inputs and vocalization in neonates. *Mef2C* suppresses corticostriatal synapse formation and striatal spinogenesis, but can, itself, be repressed by *Foxp2* through direct DNA binding. *Foxp2* deletion de-represses *Mef2C*, and both intrastriatal and global

Users may view, print, copy, and download text and data-mine the content in such documents, for the purposes of academic research, subject always to the full Conditions of use:[http://www.nature.com/authors/editorial\\_policies/license.html#terms](http://www.nature.com/authors/editorial_policies/license.html#terms)

\*Correspondence: graybiel@mit.edu (A.M.G.), fuchin@ym.edu.tw (F.-C.L.).

<sup>7</sup>Co-first author. The co-first authors are listed in alphabetical order.

Note: Any Supplementary Information and Source Data files are available in the online version of the paper.

### **AUTHOR CONTRIBUTIONS**

F.-C.L. conceived and supervised the project. Y.-C.Chen, H.-Y.K., H.T., S.-Y.C., K.-M.L., C.-T.C., U.B., W.H., W.E., S.P., A.M.G. and F.-C.L. designed the experiments. Y.-C.Chen, H.-Y.K., U.B., W.H., S.-Y.C., H.-Y.Y., G.-M.C., Y.-H. L. and S.-J.C. performed experiments on *Foxp2* and *Mef2C* mutant mice; K.-M.L., J.-R.L. and Y.-C.Chou performed *Foxp2* and *Mef2C* over-expression experiments; H.T., Y.-C.Chen and S.-Y.C. characterized *Foxp2* binding sites; W.E., S.P. provided *Foxp2* mutant mice and interpretation of data and discussion. Y.-C.Chen., H.-Y.K., S.-Y.C., K.-M.L., H.T., U.B., W.H., W.E., S.P., A.M.G. and F.-C.L. analyzed the data. A.M.G. and F.-C.L. wrote the paper with inputs from all authors.

### **COMPETING FINANCIAL INTERESTS**

We declare no competing financial interests.

decrease of *Mef2C* rescue vocalization and striatal spinogenesis defects of *Foxp2*-deletion mutants. These findings suggest that Foxp2-Mef2C signaling is critical to corticostriatal circuit formation. If found in humans, such signaling defects could contribute to a range of neurologic and neuropsychiatric disorders.

---

## INTRODUCTION

Speech and language endow human beings with unrivalled refinement and breadth in their social communications. In ASD, these communicative abilities can be severely compromised along with other problems related to social communication and repetitive behavior<sup>1</sup>. The neural mechanisms underlying language difficulties in ASD individuals present a challenge to neuroscientists<sup>2</sup>, but neuroimaging studies have detected aberrant neuronal activity and connectivity in the neocortex and striatum of ASD individuals<sup>3,4</sup>. We were struck by the parallels between these findings in ASD individuals and findings linking mutations of the *FOXP2* gene to spoken language disabilities. In both, corticostriatal dysfunction has been found along with the behavioral problems in humans and in mutant mouse models<sup>5-9</sup>. We therefore sought for signaling pathways within corticostriatal circuits that could link these two functional domains.

Human *FOXP2* has been shown to interact with several known ASD-risk genes, including *CNTNAP2*, *MET* and *uPAR*<sup>10-12</sup>, but what links *FOXP2* and these ASD-risk genes to specific neural circuits with defined neurological functions has not been clear. Nor is it known how such interactions could alter the development of language-related circuits in ASD brains. Given the potential involvement of the striatum in both ASD and language dysfunction, we searched for evidence that might link influences of ASD-risk genes and language-linked *Foxp2* during postnatal striatal development, a time of particular vulnerability in ASD. We focused on ASD candidate genes associated with synapse formation, at risk in ASD<sup>13,14</sup>. We chose for study *myocyte enhancer factor 2C* (*MEF2C*), suggested to be a possible ASD risk gene<sup>15-17</sup>, identified as one of 175 *FOXP2* targets identified by chromatin immunoprecipitation (ChIP)-chip analysis of human basal ganglia during development<sup>18</sup>, and known to be a mental retardation risk gene<sup>19</sup>. *Mef2C* has been shown to regulate negatively dendritic spines and excitatory synapses in hippocampal neurons and in cultured striatal neurons<sup>20-23</sup>. Here, we demonstrate that *Mef2C* also negatively regulates synaptogenesis in the striatum *in vivo*, but that negative interactions between *Foxp2* and *Mef2C* lead to repression of the effects of *Mef2C* coinciding spatially and temporally with the development of corticostriatal connections during early postnatal development. We show that *Foxp2* can suppress *Mef2C* through direct DNA binding, and that the negative Foxp2-Mef2C signaling interactions have specific synaptic and behavioral effects including control of ultrasonic vocalizations (USVs) in young mouse pups. We suggest that negative Foxp2-Mef2C interactions could allow cortical fibers to synapse progressively onto striatal neurons, thus building the corticostriatal pathway by de-repression of synaptogenesis in the striatum. Such Foxp2-Mef2C signaling could provide a valuable model for identifying candidate molecular mechanisms underlying developmental defects in corticostriatal circuits.

## RESULTS

### Progressive dissociation of striatal Foxp2 and Mef2C

We performed immunostaining for Mef2C and Foxp2 in the mouse brain with antibodies validated by the absence of corresponding immunofluorescent signals in Mef2C and Foxp2 knockout striatum (Supplementary Fig. 1a–f). Mef2C and Foxp2 were co-localized in many individual striatal projection neurons (SPNs) at birth, but their expression patterns soon became complementary and non-overlapping (Figs. 1 and 2). This inverse patterning was first evident in the striosome compartment of the striatum, where we found the earliest incoming corticostriatal terminals as marked by vesicular glutamate transporters 1 (VGluT1; Fig. 1a). During the early postnatal (P) period, P0–P4, striosomes, marked by DARPP-32, were nearly devoid of Mef2C, despite strong Mef2C expression in the surrounding matrix (Figs. 1b and 2d). Strong Foxp2 expression, by contrast, was found in striosomes (Fig. 1). By P8 and P14, the inverse expression patterns of Foxp2 and Mef2C had extended across the striatum (Fig. 2b,c,f), paralleled by a progressive expansion of the corticostriatal innervation from the striosomes to the entire striatum (Fig. 2a–c)<sup>24</sup>, dorsolateral expansion leading slightly (Fig. 2g). This striking progression from co-localization to dissociation of Mef2C and Foxp2 expression coincided with the postnatal time-period during which corticostriatal axonal collaterals arborize and the dendritic spines of SPNs develop<sup>24–26</sup>, suggesting that Mef2C and Foxp2 might oppositely regulate corticostriatal synapse formation.

### Foxp2 and Mef2C inversely control corticostriatal synaptogenesis

To examine the relationship of Foxp2 and Mef2C expression to the development of the corticostriatal projection system, we analyzed synaptogenesis in *Mef2C* knockout (*Nestin-Cre;Mef2C<sup>fl/fl</sup>*)<sup>21</sup> and *Foxp2* knockout (*Foxp2<sup>-/-</sup>*)<sup>8</sup> mice, and also in *Foxp2* humanized (*Foxp2<sup>H/H</sup>*) mice<sup>8</sup> as a gain-of-function model. We identified corticostriatal synapses with VGluT1 as a pre-synaptic marker<sup>27</sup> and postsynaptic density protein 95 (PSD-95) and glutamate receptor 1 (GluR1) as post-synaptic markers (Supplementary Fig. 1g). We focused on P12–P14, by which time Foxp2 was expressed throughout the striatum and Mef2C was nearly absent except far medially (Fig. 2h).

In the *Foxp2<sup>-/-</sup>* knockout mice, western blots of striatal VGluT1 and PSD-95 proteins and immunostaining of striatal GluR1 showed that these synaptic markers all were reduced relative to those in wildtype mice (Fig. 3a and Supplementary Fig. 2a–c), but these markers were increased in the humanized *Foxp2<sup>H/H</sup>* striatum (Fig. 3b and Supplementary Fig. 2d–f), suggesting that Foxp2 positively regulates striatal synaptogenesis. By contrast, *Mef2C* negatively regulated striatal synaptogenesis. VGluT1 and PSD-95 proteins and GluR1 immunostaining significantly increased in the striatum of *Nestin-Cre;Mef2C<sup>fl/fl</sup>* conditional *Mef2C* knockout mice relative to control *Nestin-Cre;Mef2C<sup>+/+</sup>* mice (Fig. 3c and Supplementary Fig. 2g–i). Thus, Foxp2 and Mef2C had opposite effects on synaptogenesis in the developing striatum.

Markers of striosomes ( $\mu$ -opioid receptor 1, MOR1) and of the matrix (calcium and diacylglycerol-guanine nucleotide exchange factor I, CalDAG-GEFI) showed that striosome-matrix compartmentation was maintained in the three genotypes (Supplementary Fig. 3a–f).

No abnormal cell death was found in P0 or P8 *Foxp2*<sup>-/-</sup> knockouts, nor in *Nestin-Cre;Mef2C*<sup>fl/fl</sup> knockout mice at embryonic day (E) 18.5 and P8, as assayed by TUNEL staining and immunostaining for activated caspase3 (Supplementary Fig. 3i-r). The alterations in synaptic markers were thus likely not secondary to loss of compartmentation or to widespread cell death in the mutant mice.

### ***Foxp2* and *Mef2C* oppositely regulate SPN spinogenesis**

The dendritic spines of striatal SPNs are the main sites of corticostriatal synapses. We examined the development of these synapses in the three mouse genotypes (Fig. 3d-f, Supplementary Fig. 4 and Supplementary Table 1-3). Golgi-staining in P12 *Foxp2*<sup>-/-</sup> knockout mice showed reductions in the total spine density of SPNs of 14.0% dorsolaterally and 19.1% dorsomedially (Fig. 3d, Supplementary Fig. 4a and Supplementary Table 1). In heterozygous *Foxp2*<sup>+/-</sup> mice, only the most mature spine types<sup>28</sup> were reduced (Fig. 3d, Supplementary Fig. 4a and Supplementary Table 1), a finding potentially relevant to pathophysiology in KE patients, who carry heterozygous *FOXP2*<sup>R553H</sup> missense mutations<sup>9</sup>. In the positive control mice carrying humanized *Foxp2*<sup>H/H</sup>, SPN spine densities were increased both dorsolaterally and dorsomedially relative to those in wildtype littermates (Fig. 3e, Supplementary Fig. 4b and Supplementary Table 2). We microinjected HSV-Cre-GFP viruses into the striatum of P2 *Foxp2*<sup>H/H</sup> mice carrying floxed human versions of *Foxp2* alleles<sup>8</sup>. Immunostaining demonstrated a loss of Foxp2 protein expression in HSV-Cre-GFP virus-infected cells (Supplementary Fig. 5d-e), and this postnatal deletion of *Foxp2*<sup>H/H</sup> decreased spines by 68% in HSV-Cre-GFP virus-infected SPNs at P8 (Fig. 3g). These findings suggested that Foxp2 positively regulated synaptogenesis, but that Mef2C negatively regulated synaptogenesis, as found in hippocampal neurons<sup>20-22</sup>.

We used *in utero* electroporation to over-express mouse *Foxp2* gene in wildtype striatal cells. Introduction of Foxp2 plasmid co-expressing enhanced yellow fluorescent protein (EYFP) into the E13.5 striatal primordium increased dendritic spine numbers as tested by EYFP/GFP immunostaining of P14 SPNs (Fig. 3h). Conversely, spine density was significantly increased in striatal SPNs in *Nestin-Cre;Mef2C*<sup>fl/fl</sup> conditional knockouts relative to control *Nestin-Cre;Mef2C*<sup>+/+</sup> mice for all but the least mature subtypes (Fig. 3f, Supplementary Fig. 4c and Supplementary Table 3).

We also microinjected HSV-Cre-GFP virus into the striatum of P2 *Mef2C*<sup>fl/fl</sup> pups and examined their brains at P8. Immunostaining confirmed loss of Mef2C protein expression in HSV-Cre-GFP virus-infected cells (Supplementary Fig. 5a-c) and indicated significant increases in spine counts in the HSV-Cre-GFP virus-infected SPNs (Fig. 3i). Intrastriatal injection of HSV-Cre-GFP viruses in *Mef2C*<sup>fl/fl</sup> mice at P14-15, when Mef2C expression already was low (Fig. 2h), showed no detectable changes in dendritic spines of SPNs at P19-P20 (Fig. 3j). Finally, we over-expressed *Mef2C* by *in utero* electroporation of pcBIG-Mef2C-VP16 plasmids into the E12.5 striatal primordium of wildtypes. This procedure decreased the number of spines in P14 SPNs (Fig. 3k). These findings identify Mef2C as a negative regulator of spine and synapse formation in SPNs of the developing postnatal striatum, consonant with *in vitro* work on Mef2-class proteins<sup>23</sup>.

In slice preparations, we analyzed miniature excitatory postsynaptic currents (mEPSCs) of dorsolateral SPNs in *Foxp2<sup>H/H</sup>*, *Foxp2* knockout, and *Nestin-Cre;Mef2C<sup>f/f</sup>* knockout brains relative to their wildtype controls. Whole-cell patch-clamp recordings indicated an increase in mEPSC frequency in 36.2% of SPNs in P14 *Foxp2<sup>H/H</sup>* mice without significant change in mEPSC amplitudes (Fig. 3l). In P8 *Foxp2<sup>-/-</sup>* knockout mice, mEPSC frequency was decreased in SPNs, but mEPSC amplitude was increased compared to wildtype (Fig. 3m). In P14 *Nestin-Cre;Mef2C<sup>f/f</sup>* knockout brains, mEPSC frequency, but not amplitude, was increased in SPNs relative to control *Nestin-Cre;Mef2C<sup>+/+</sup>* mice (Fig. 3n). These findings demonstrated that synaptic activity in striatal SPNs is positively regulated by *Foxp2*, but negatively regulated by *Mef2C*, consistent with our anatomical findings (Fig. 3, Supplementary Fig. 4 and Supplementary Tables 1–3).

### **Foxp2 suppresses Mef2C expression in striatal SPNs**

The opposing functions of *Mef2C* and *Foxp2* in regulating corticostriatal synapse formation and SPN spinogenesis, and their striking spatiotemporal dissociation during neonatal development, suggested that the positive regulation of spine and synapse formation in striatal SPNs by *Foxp2* might depend on its ability to suppress *Mef2C*. As an initial probe for this potential interaction, we asked whether the near-absence of *Mef2C* expression in striosomes in the normal neonatal striatum could be reversed by deletion of *Foxp2*. We found striking de-repression of *Mef2C* expression in striosomes in the P7 *Foxp2<sup>-/-</sup>* striatum (Fig. 4a,b) with the striosome predominance of immunofluorescence intensity of *Mef2C*–positive cells increased in the *Foxp2<sup>-/-</sup>* knockout mice compared to levels in wildtypes (Fig. 4c). In western blots, *Mef2C* protein levels were increased by 68.3% over control levels in the P12 *Foxp2<sup>-/-</sup>* striatum (Fig. 4d) and were decreased in P14 *Foxp2<sup>H/H</sup>* mice (Fig. 4e). In quantitative real-time polymerase chain reaction (qRT-PCR) assays, *Mef2C* mRNA was increased in *Foxp2<sup>-/-</sup>* knockout striatum (Fig. 4f), but decreased in the *Foxp2<sup>H/H</sup>* striatum (Fig. 4g). *In vitro* over-expression of *Foxp2* in Neuro2A (N2A) cells was sufficient to decrease *Mef2C* protein by 23.5% (Fig. 4h). These findings were consistent with an antagonism of *Mef2C* by *Foxp2* in the striatum. *Mef2C* was persistently expressed in neocortex of postnatal wildtype mice (Supplementary Fig. 1h–j). We found no changes in *Mef2C* protein levels or *Mef2C*–positive cell numbers in the neocortex of P8 *Foxp2<sup>-/-</sup>* knockouts (Supplementary Fig. 6a–d).

We tracked striatal *Mef2C* and *Foxp2* protein levels by western blot analysis from P4 to P21. For *Foxp2* knockout striatum at P4, the levels of *Mef2C* and the synaptic markers VGluT1, PSD-95 and GluR1 were not different from controls (Supplementary Fig. 6e), but by P8, there was a significant increase of *Mef2C* and significant decreases of VGluT1, PSD-95 and GluR1 (Supplementary Fig. 6f), patterns maintained at P12 (Supplementary Fig. 6g). In the humanized *Foxp2* striatum, *Mef2C* was decreased, and VGluT1 and GluR1 were increased as early as P4 relative to controls (Supplementary Fig. 6h) and remained elevated at P8 and P21 (Supplementary Fig. 6i,j). These results delineated consistent negative interactions of *Foxp2* and *Mef2C* in their effects on striatal synaptogenesis detectable around P4–P8 and persisting for at least 3 postnatal weeks, suggesting that *Foxp2* could act to repress *Mef2C* expression in the striatum.

### ***Mef2C* is a direct downstream target gene of *Foxp2***

One mechanism by which repression of *Mef2C* by *Foxp2* could occur would be if the *Mef2C* gene were to contain the canonical FOXP2 binding site “CAAATT” and the binding site core, “AAAT”<sup>18</sup>. *Foxp2* binds to DNA by dimerization<sup>29</sup>. We found two pairs of putative *Foxp2* binding sites in the second intron of the *Mef2C* gene [ACAAAT (–1948 bp) & AAAT (–1935 bp); and AAAT (–1837 bp) & CAAATT (–1788 bp); translational initiation site A+1TG; Fig. 5a]. With ChIP-quantitative PCR (ChIP-qPCR) assays of mouse striatal cells at E16, we found that *Foxp2* antibody, but not control IgG antibody, immunoprecipitated a DNA fragment containing the two pairs of *Foxp2* motifs (Fig. 5b). Thus, *Foxp2* can bind directly to this region containing the canonical *Foxp2* binding motifs *in vivo*.

We cloned this DNA region into a pGL3-c-fos-Luciferase (Luc) reporter gene construct and co-transfected into N2A cells the *Mef2C*–pGL3-c-fos-Luc plasmid with a *Foxp2* expression plasmid. Transfection of the mouse *Foxp2* gene repressed Luc activity by 29% compared to mock controls (Fig. 5c). Transfection of the human *FOXP2* gene, but not the *hFOXP2*<sup>R553H</sup> mutant lacking DNA binding capacity, resulted in a similar (31%) decrease of Luc activity (Fig. 5c).

We next mutated the sequences of the ACAAAT and AAAT motifs to ACGGGT & GGGT (MT1), and the sequences of the AAAT & CAAATT motifs to GGGT & CGGGTT (MT2) by site-directed mutagenesis. The repression of Luc reporter gene activity was abolished when either *Mef2C*–MT1-c-fos-Luc or *Mef2C*–MT2-c-fos-Luc mutant plasmid was co-transfected with mouse *Foxp2* expression plasmid (Fig. 5c). Loss of repression of Luc activity also occurred with co-transfection of human *FOXP2* gene and the MT1 or MT2 mutant reporter gene constructs (Fig. 5c). These results suggest that *Foxp2* directly binds to the two canonical *Foxp2* binding motifs to repress functionally the capacity for *Mef2C* gene expression.

We looked for, and identified, putative FOXP2 binding motifs in the promoter region of the human *MEF2C* gene (Supplementary Fig. 7), a finding potentially linking our mouse work to the suggestion that human *MEF2C* gene is a putative target gene of FOXP2 in human embryonic basal ganglia tissue<sup>18</sup>.

### ***Mef2C* deletion rescues USVs and SPN spines in *Foxp2*<sup>+/-</sup> mice**

*Foxp2* heterozygous and homozygous knockout mice exhibit defective neonatal isolation-induced USVs<sup>30</sup>, a form of vocal communication in neonatal rodents. Our finding that *Mef2C* is normally repressed by *Foxp2* suggested that, by reducing abnormally overactive *Mef2C* in *Foxp2* knockouts, we might be able to rescue such defective USV in *Foxp2* mutants. If so, this link would constitute functional evidence for an interaction of the two proteins in vocal communication.

We tested this possibility in *Foxp2*<sup>+/-</sup> heterozygotes, mouse models of humans carrying one allele of the *FOXP2* mutation. We confirmed that these *Foxp2*<sup>+/-</sup> mutants had abnormal USVs (Supplementary Fig. 8a) and then examined the effects of inactivation of one allele in *Mef2C*<sup>fl/fl</sup>, accomplished by genetic introduction of striatum-enriched *Dlx5/6-Cre* in *Dlx5/6*–

*Cre;Foxp2<sup>+/-</sup>;Mef2C<sup>fl/+</sup>* mice. This partial inactivation of Mef2C significantly rescued many features of the abnormal USVs characteristic of P8 *Foxp2<sup>+/-</sup>* mice, as compared to USVs of control P8 *Dlx5/6-Cre;Foxp2<sup>+/-</sup>;Mef2C<sup>+/+</sup>* mice (Fig. 6a–d and Supplementary Fig. 8b). The fact that we found no marked differences in USV features between *Dlx5/6-Cre;Foxp2<sup>+/+</sup>;Mef2C<sup>fl/+</sup>* mice, which had normal *Foxp2* but a deleted *Mef2C* allele, and *Dlx5/6-Cre;Foxp2<sup>+/+</sup>;Mef2C<sup>+/+</sup>* mice, which had normal *Foxp2* and normal *Mef2C* alleles, ruled out the possibility that the effect of Mef2C reduction was mediated through a pathway independent of *Foxp2* (Supplementary Fig. 8c).

The single-allele genetic reduction of *Mef2C* levels also significantly rescued VGlut1 and PSD-95 protein levels in the striatum of *Mef2C*-deficient *Dlx5/6-Cre;Foxp2<sup>+/-</sup>;Mef2C<sup>fl/+</sup>* mice compared to those in control *Dlx5/6-Cre;Foxp2<sup>+/-</sup>;Mef2C<sup>+/+</sup>* mice (Fig. 6e). SPN spine counts were markedly increased dorsolaterally and dorsomedially (Fig. 6f, Supplementary Fig. 4d and Supplementary Table 4). These synaptic rescue effects were evident in both striosome and matrix compartments, judging by significantly increased immunostaining for GluR1 (Fig. 6g–i).

To test the possibility that the spine rescue occurred because of general effects of genetic deletion on development, we restricted deletion of *Mef2C* specifically in the neonatal striatum by intrastriatal microinjection of HSV-Cre-GFP virus of P2 *Foxp2<sup>+/-</sup>;Mef2C<sup>fl/+</sup>* pups and performing GFP immunostaining and Golgi assays at P8. This striatum-specific decrease of Mef2C resulted in significant increases in dendritic spines in HSV-Cre-GFP virus-infected SPNs of *Foxp2<sup>+/-</sup>;Mef2C<sup>fl/+</sup>* mice compared to the spines of SPNs in control *Foxp2<sup>+/-</sup>;Mef2C<sup>+/+</sup>* mice (Fig. 6j). The USV events and frequency-jump scores of the pups were also rescued in the HSV-Cre-GFP;*Foxp2<sup>+/-</sup>;Mef2C<sup>fl/+</sup>* pups (Fig. 6k,l and Supplementary Fig. 8d).

These multiple lines of evidence directly suggest that corticostriatal synaptic protein levels are suppressed by Mef2C and can be co-rescued along with behavioral rescue of USVs by expression of *Foxp2*. These findings suggest that *Mef2C* acts downstream of *Foxp2* to regulate synaptic wiring of corticostriatal circuits that contribute to vocalization.

### USV deficits occur in *Mef2C* knockout mice

Conditional *Mef2C* knockout (*Nestin-Cre;Mef2C<sup>fl/fl</sup>*) mice exhibit autistic-like behavioral phenotypes, putatively murine counterparts of Rett syndrome features, including increased anxiety, decreased cognition and paw wringing/clasping stereotypy<sup>31</sup>. It remained unclear whether such *Nestin-Cre;Mef2C<sup>fl/fl</sup>* mice displayed deficits in vocal communication. Because our rescue experiments suggested that *Mef2C* acts downstream of *Foxp2* to regulate USVs (Fig. 6a–d,k-l), we expected that deletion of *Mef2C* would alter USVs. We tested this possibility and found that the numbers of emitted USVs were significantly reduced in the *Nestin-Cre;Mef2C<sup>fl/fl</sup>* mice, compared to those in control *Nestin-Cre;Mef2C<sup>+/+</sup>* mice (Fig. 7a), and that the deficit included significant reductions in many USV features (Fig. 7a–d,j), though some USV features were unaffected (Fig. 7e–i). Thus *Mef2C* deletion can result in a deficit in USVs, a vocalization-like phenotype, adding evidence consistent with the working proposal, made here, that *Foxp2*-*Mef2C* signaling could regulate vocalization along with regulating corticostriatal connectivity.

## DISCUSSION

Our findings provide causal evidence that Mef2C is directly implicated in the conjoint deleterious behavioral and morphological effects of reductions in Foxp2. We demonstrate that Mef2C is a negative regulator of synapse formation in the projection neurons of the developing striatum, and that Mef2C expression is itself a direct target of gene suppression by the *Foxp2* gene in these neurons (Supplementary Fig. 9). Thus Foxp2, by negatively regulating Mef2C, can promote the formation of the massive corticostriatal connectivity that is known to be functionally important in behavior.

Our findings suggest that Foxp2 acts in the early postnatal period by coordinately promoting corticostriatal synaptogenesis and retarding the expression of Mef2C in the striatum. Deletion of Foxp2 increased neonatal striatal Mef2C expression and, in parallel, decreased corticostriatal synaptogenesis and spinogenesis of striatal SPNs. Engineered expression of humanized Foxp2 in mouse had opposite effects on the developing corticostriatal circuits and striatal neurons. Our evidence that canonical Foxp2 binding sites are required for the Foxp2 inhibition of Mef2C expression suggests that there are direct molecular interactions between Foxp2 and Mef2C. We found that intrastriatal as well as genome-wide decreases in Mef2C can rescue defects in USVs and striatal spinogenesis otherwise occurring in *Foxp2* mutants. Finally, our study of USVs suggests that these Foxp2-Mef2C interactions exert orchestrated control over corticostriatal systems affecting social vocalization in neonates. Our findings are based on mouse models, and so might not be relevant to clinical conditions. Given that *MEF2C* has been suggested to be an ASD candidate risk gene and is known to be a gene related to mental retardation<sup>15–17,19</sup>, and that *FOXP2* has been identified as a language-associated gene<sup>9</sup>, a plausible hypothesis raised by our findings is that the Foxp2-Mef2C interactions we demonstrate here, and their profound effects on corticostriatal circuitry, could be relevant to mechanisms underlying spoken language dysfunction in ASD. More generally, such interactions, controlling the development of the corticostriatal system, could be relevant to a range of normal and abnormal functions in which this massive corticostriatal circuitry has been implicated clinically, notably including Huntington's disease.

### Foxp2-Mef2C control of USVs and corticostriatal circuit

The potential behavioral significance of interactions between Foxp2 and Mef2C was demonstrated by assays of USVs in mice that lacked one allele of *Foxp2* and one allele of *Mef2C* (*Dlx5/6-Cre;Foxp2<sup>+/-</sup>;Mef2C<sup>fl/+</sup>* mice). Genetic reduction of *Mef2C* levels rescued four of the seven USV defects exhibited by *Foxp2* heterozygotes and increased VGlut1 and PSD-95 synaptic proteins in the striatum, relative to levels of the corresponding proteins in control *Dlx5/6-Cre;Foxp2<sup>+/-</sup>;Mef2C<sup>+/+</sup>* mice. The USV and spine formation deficits were also partially rescued by selective early postnatal reduction of Mef2C. While not ruling out other contributions, these findings support the striatal specificity of Foxp2-Mef2C interactions in regulating synaptogenesis in SPNs and vocalization behavior of the pups. We also found a clear correlation between synaptic alterations in *Dlx5/6-Cre;Foxp2<sup>+/-</sup>;Mef2C<sup>+/+</sup>* mice (*Foxp2* heterozygotes) and the USV deficits in these mice, further linking anatomical and functional control by Foxp2-Mef2C signaling.



## Foxp2 as a molecular key to unlock Mef2C–induced inhibition

Our findings demonstrate that interactions between *Foxp2* and *Mef2C* are required for establishing the normal synaptic connectivity of corticostriatal circuits. In the hippocampus, Mef2 protein interacts with the ASD-risk genes, *FMRP* and *Pcdh10*, to induce degradation of PSD-95 protein for elimination of excitatory synapses<sup>22</sup>. This work suggests a central role for Mef2 in negative regulation of hippocampal synapses. Our findings identify Foxp2 as a molecular key to unlock the inhibition of striatal synapse formation imposed by Mef2C, thereby allowing the initiation of synaptic connectivity of corticostriatal circuits within the striatum. Our data support a postnatal role, as early as P2, for Foxp2-mediated repression of Mef2C in the regulation of spinogenesis. As spines start to grow in postnatal SPNs, Mef2C, which inhibits spine formation, presumably must be down-regulated to permit the progression of spine formation in SPNs. The gradual decrease in Mef2C in the postnatal striatum and the maintenance of these low levels at least until P14 are consistent with this hypothesis. The evidence of increased spine formation in SPNs by postnatal deletion of *Mef2C* gene at P2 further supports this working model. Our experiments did not clarify whether Mef2C acts to prune exuberant striatal SPN synapses or to inhibit synapse formation in these SPNs. However, given our observation that Mef2C is strongly expressed in striatal matrix SPNs before these SPNs are innervated by corticostriatal axon terminals in newborn striatum (Fig. 1b), an intriguing possibility is that Mef2C functions as a molecular gate to prevent immature synapse formation unless it is triggered by an appropriate input. This gate-control role for Mef2C would suggest that a rigorously timed and specific molecular mechanism is implemented for developmental control of synaptic wiring of corticostriatal circuits. We suggest that Foxp2 inhibition of Mef2C could provide such a mechanism, potentially through direct DNA binding of Foxp2 to *Mef2C*, and that defects in this inhibition by Foxp2 could have deleterious effects.

ChIP-chip analysis has identified *MEF2D* in addition to *MEF2C* as potential target genes of *FOXP2* in embryonic human brains<sup>18</sup>. For other members of *Mef2* family, in contrast to the low levels of Mef2C in the mature striatum, levels of Mef2D and Mef2A are high in the mature mouse striatum, where they have been implicated in the plasticity of dendritic spines in SPNs induced by exposure to cocaine<sup>32</sup>. In the hippocampus, dendritic spine formation is negatively regulated by *Mef2C* in the dentate gyrus of *hGFAP-Cre;Mef2C* mice<sup>21</sup>, but not in the CA1 region of *hGFAP-Cre;Mef2A;Mef2D* double-knockout mice or *hGFAP-Cre;Mef2A;Mef2C;Mef2D* triple-knockout mice, apparently reflecting low Mef2C expression in the CA1 region<sup>33</sup>. Postnatal deletion of *Mef2C* also results in increased spines in the dentate gyrus in *CaMKII-Cre;Mef2C* knockout mice<sup>34</sup>.

## Comparison of *Foxp2* in striatal and cortical synaptogenesis

In contrast to the developmental down-regulation of Mef2C in postnatal striatum, Mef2C was persistently expressed in postnatal neocortex of wildtype mice. Our finding that Mef2C protein was not altered in the neocortex of *Foxp2* knockout mice suggests that Foxp2-Mef2C interaction does not dominate the development of cortical neurons, but leaves open the possibility of some compensatory mechanism in the neocortex. In cultured neocortical neurons, *Foxp2* has been found to regulate negatively excitatory synaptogenesis via inhibition of *SPRX2*, an epilepsy- and language-associated gene<sup>35</sup>. The positive action of

Foxp2-Mef2C signaling on synaptogenesis in the striatum, shown here, and the reported negative action of Foxp2-SPRX2 signaling on synaptogenesis in cortical neurons, suggest a commanding and highly differentiated role for *Foxp2* in developmental control of neural circuits that have been related to language. In the avian model of vocal communication, knocking down songbird *FoxP2* in Area X decreases spine density in neurons of Area X and decreases vocal motor learning<sup>36,37</sup>. Our findings add to evidence for a controlling role for Foxp2, explicitly by introducing its ability to suppress Mef2C as a potential critical mechanism contributing to the control of vocalization.

### Potential clinical relevance of Foxp2-Mef2C interactions

Our findings suggest a molecular mechanism by which *Foxp2* can regulate excitatory corticostriatal synapses onto striatal projection neurons in mice through suppression of *Mef2C*, whose progressive down-regulation is synchronized spatially and temporally with the development and synaptogenesis of corticostriatal circuits. Our evidence specifically suggests that *Foxp2* transcriptionally suppresses the synaptogenesis suppressor, *Mef2C*, thereby allowing corticostriatal synaptogenesis.

There is no direct evidence from our work that these interactions occur in the human brain, or that they relate to human conditions including ASD and speech and language. *FOXP2* is considered a 'language-related gene'<sup>9</sup>, but its precise relation to speech and language is still a matter of study. Similarly, *MEF2C* has been identified as a candidate ASD gene<sup>15-17</sup>, but evidence for linkage of *MEF2C* mutations to ASD is still incomplete. *MEF2C* mutations have been linked to phenotypes including mental retardation in humans<sup>15,19</sup>, a matter of current research. It is known, however, that *MEF2C* is a putative target gene of *FOXP2* in the developing human basal ganglia<sup>18</sup>, and our findings suggest that the human *FOXP2* protein is at least as effective as, or more effective than, the mouse Foxp2 protein in promoting synapse and complex spine formation in SPNs in the mouse striatum. A possibility raised by our findings is that the interactions that we have documented in the mouse hold in some form in the human. If so, our findings could be interpreted as relevant to a molecular linkage between the putative ASD candidate gene, *MEF2C*, and the putative language-associated gene, *FOXP2*. Notably, *Mef2C* is regulated by *MeCP2*, a well-established Rett syndrome gene with broad effects<sup>38</sup>, and *MEF2* is implicated in regulation of the ASD-risk genes, *DIA1* and *PCDH10*<sup>39</sup>. Thus, our findings could be relevant in the context of multiple ASD-risk genes interacting in signaling networks for neuronal development<sup>13,14</sup>.

Human patients with *MEF2C* deletion and mutation have complex neurological syndromes<sup>15,16,19</sup>. In addition to defective language communication, stereotypic behaviors, potentially linked to striosomes<sup>40</sup>, have been reported in patients with *MEF2C* deletion and mutation<sup>15,19</sup> and in the *Mef2C* knockout mouse model of ASD<sup>31,41</sup>. Our findings indicate that part of the etiology of *MEF2C*-related ASD symptoms could be rooted in the basal ganglia. We raise the possibility that defective FOXP2-MEF2C signaling affecting developing corticostriatal synaptic circuits could be a previously underestimated pathologic mechanism in conditions characterized by corticostriatal abnormalities.

## ONLINE METHODS

### Animals

*Foxp2*<sup>+/-</sup> mice and humanized *Foxp2*<sup>H/+</sup> mice were generated as previously described<sup>8</sup>. *Mef2C*<sup>fl/+</sup> mice (kindly provided by Dr. Eric Olson) were generated as previously described<sup>21</sup>. All mice were maintained with freely available food and water in a specific pathogen-free room with a constant humidity and 12-hr light-dark cycle (2–3 adult mice/cage; 6–8 pups/cage) in the animal center of National Yang-Ming University. All the experiments on single *Foxp2* mutant mice were performed on littermate mice derived from the offspring of crosses between heterozygous *Foxp2*<sup>+/-</sup> x *Foxp2*<sup>+/-</sup> or *Foxp2*<sup>H/+</sup> x *Foxp2*<sup>H/+</sup> mice. *Nestin-Cre* mice<sup>42</sup> were crossed with *Mef2C*<sup>fl/+</sup> mice to derive *Nestin-Cre;Mef2C*<sup>fl/+</sup> mice. *Nestin-Cre;Mef2C*<sup>fl/+</sup> mice were then crossed with *Mef2C*<sup>fl/fl</sup> mice to generate *Nestin-Cre;Mef2C*<sup>fl/fl</sup> conditional knockout mice. *Foxp2*<sup>+/-</sup> mice were crossed with *Mef2C*<sup>fl/fl</sup> mice to derive *Foxp2*<sup>+/-</sup>;*Mef2C*<sup>fl/+</sup> mice. *Dlx5/6-Cre* mice<sup>43</sup> were crossed with *Foxp2*<sup>+/-</sup>;*Mef2C*<sup>fl/+</sup> mice to derive *Dlx5/6-Cre;Foxp2*<sup>+/-</sup>;*Mef2C*<sup>fl/+</sup> mice. *Dlx5/6-Cre;Foxp2*<sup>+/-</sup>;*Mef2C*<sup>fl/+</sup> mice were then crossed with *Foxp2*<sup>+/-</sup>;*Mef2C*<sup>fl/+</sup> mice. *Foxp2*<sup>+/-</sup>, *Foxp2*<sup>H/+</sup>, *Mef2C*<sup>fl/+</sup> and *Nestin-Cre* mice were maintained in C57Bl/6 genetic background. *Dlx5/6-Cre* mice were maintained in CD-1 background. We used both genders for experiments. All animal protocols were approved by the Animal Care and Use Committees of National Yang-Ming University.

### Genotyping

Genotyping was performed by PCR with the genomic DNA. Tissues for the genotyping were collected, and then were incubated overnight in DNA lysis buffer (10 mM Tris, 10 mM EDTA, 100 mM NaCl, 0.5% SDS, 250 µg/ml protease K) at 55°C. After incubation, lysates were treated with RNase A for 30 min at 37°C, followed by addition of 200-µl protein precipitation solution (Promega), and they were kept on ice for 1 hr to separate proteins and RNA from genomic DNA. Finally, the genomic DNA was extracted by isopropanol (1:1), washed with 500 µl of 70% ethanol and placed overnight in 100 µl of Tris-EDTA buffer at 37°C to dissolve. For PCR genotyping, three primers were used to detect the *Foxp2* mice genotypes: *Foxp2*ko\_5425\_f (5'-TTCTCTCCTGTCTCCCATTGA-3'), *Foxp2*ko\_8502\_f (5'-CACGCCAGCTACATTTTAA-3'), and *Foxp2*ko\_8729\_r (5'-GCAGAAACACTATGGTGGGAAG-3'). The PCR product derived from *Foxp2*ko\_5425\_f/*Foxp2*ko\_8729\_r was 194 bp in wildtype mice; and that from *Foxp2*ko\_8502\_f/*Foxp2*ko\_8729\_r was 350 bp in *Foxp2*<sup>-/-</sup> knockout mice. The PCR product derived from *Foxp2*ko\_8502\_f/*Foxp2*ko\_8729\_r was 228 bp in humanized *Foxp2*<sup>H/H</sup> mice. The primers used for detecting genotypes of the *Mef2C*<sup>fl/+</sup>, *Nestin-Cre* and *Dlx5/6-Cre* mice were as follows:

*Mef2C*-5' (5'-  
GTGATGACCCATATGGGATCTAGAAATCAAGGTCCAGGGTCAG-3'),  
*Mef2C*-3' (5'-  
CTACTTGTCCCAAGAAAGGACAGGAAATGCAAAAATGAGGCAG-3'),  
*Nestin* (*Dlx5/6*)-*Cre*-5' (5'-GCTAAACATGCTTCATCGTCCG-3'),

and Nestin (Dlx5/6)-Cre-3' (5'-GATCTCCGGTATTGAAACTCCAGC-3').

The PCR genotyping protocols were as follows: 94°C for 5 min, 35 cycles at 94°C for 30 s, 58°C (Foxp2, Nestin-Cre, Dlx5/6-Cre) or 65°C (Mef2C) for 30 s, and 72°C for 30 s. Finally, an additional step was run at 72°C for 5 min before completing the PCR reaction.

### ***In utero* electroporation**

The pCAG-EYFP-CAG-Foxp2, pCAG-EYFP-CAG, pcBIG-Mef2C-VP16 (Mef2C-VP16 cDNA kindly provided by E. Olson) and pcBIG (vector kindly provided by P. Arlotta) plasmids were prepared using an endotoxin-free kit (Novelgene) and were injected (1.5 µl, 2 µg/µl) into the lateral ventricle of E12.5 (pcBIG-Mef2C-VP16, pcBIG) or E13.5 (pCAG-EYFP-CAG-Foxp2, pCAG-EYFP-CAG) forebrains of wildtype mouse embryos followed by electroporation (7 pulses, 33 V, 30 ms duration, 970 ms interval; BTX ECM 830). The electroporated mice were born and were perfused at P14 for GFP immunostaining.

### **Virus transduction**

ST HSV-Cre-GFP viruses (Viral Core Facility, McGovern Institute for Brain Research, MIT) were diluted 1:1 in D-PBS buffer. *Foxp2*<sup>+/+</sup>, *Foxp2*<sup>H/H</sup>, *Mef2C*<sup>+/+</sup>, *Mef2C*<sup>fl/fl</sup>, *Foxp2*<sup>+/-</sup>; *Mef2C*<sup>+/+</sup> and *Foxp2*<sup>+/-</sup>; *Mef2C*<sup>fl/+</sup> mouse pups were anesthetized by hypothermia at P2, and virus solution (0.2 µl) was injected (0.1 µl/min) bilaterally in the rostral (AP: +2.85 mm, ML: ±1.60 mm, DV: -1.80 and -2.00 mm) and middle (AP: +2.55 mm, ML: ±1.51 mm, DV: -1.50 and -1.70 mm) striatum. After injections, the needle was left for 2 min before slow retraction. A few pups received injections only at the middle striatum. The pups were allowed to survive until P8, and following perfusion, the brains were prepared for Golgi staining and immunostaining. In another set of experiments, intrastriatal viral injections were made in *Mef2C*<sup>fl/fl</sup> mice at P14–15 at rostral (AP: + 3.75 mm, ML: ±2.20 mm, DV: -2.5 and -2.8 mm) and middle (AP: +3.33 mm, ML: ±2.35 mm, DV: -3.0 and -3.5 mm) levels. The brains were harvested at P19-P20.

### **Preparation of brain tissue**

For western blotting analysis, P4, P8, P12, P14 and P21 mice were deeply anesthetized by intraperitoneal injection of sodium pentobarbital, and brains were cut into 1 mm coronal slices using acrylic brain slice matrix (Alto). The selected slices containing the regions of interest were then frozen with dry ice and used for analysis. For immunohistochemical analysis, P0, P4, P7, P8, P14 and P30 mice were perfused transcardially with 0.9% saline followed by 4% paraformaldehyde (PFA) in 0.1 M phosphate buffered saline (PBS, pH 7.4). The perfused brains were post-fixed in 4% PFA at 4°C overnight and were then cryoprotected with 30% sucrose in 0.1 M PBS. Brains were cut in the coronal plane on a cryostat at 20 µm (Lecia).

### **Golgi staining**

P12 and P14 brain tissues were prepared and processed for Golgi staining using the FD Rapid GolgiStain Kit (FD NeuroTechnologies) according to the manufacturer's instruction. Transverse sections were cut at 80 µm on a cryostat (Lecia). P8 brains infected with HSV-

Cre-EGFP viruses were processed using the sliceGolgi Kit (Bioenno Tech) for double Golgi staining and GFP immunostaining with DAB substrate.

### Immunohistochemistry

Immunohistochemistry was performed as previously described<sup>44</sup>. Primary antibodies were as follows: rabbit anti-Foxp2 (1:2,000; #ab16046, Abcam), rabbit anti-MOR1 (1:10,000; #24216, ImmunoStar), rabbit anti-CalDAG-GEFI (1:10,000)<sup>40</sup>, rabbit anti-GluR1 (1:2,000; #ab1504, Millipore), rabbit anti-activated caspase3 (1:1,000, #9661, Cell Signaling), rabbit anti-PSD95 (1:10; #20665-1-AP, Proteintech), goat anti-Mef2C (1:1,000; #sc-13266, Santa Cruz), guinea pig anti-VGluT1 (1:5,000; #ab5905, Millipore), mouse anti-DARPP-32 (1:10,000, kindly provided by Dr. H.C. Hemmings) and chicken anti-GFP (1:500; #ab13970, Abcam). For triple immunostaining of Foxp2, Mef2C and VGluT1, Alexa555-conjugated goat anti-rabbit antibody and Alexa647-conjugated goat anti-guinea pig antibody were used to detect Foxp2 and VGluT1 signals. For detecting Mef2C signals, sections were incubated sequentially in biotin-conjugated donkey anti-goat antibody, ABC complex (ABC kit, Vector Laboratories) and tyramide-FITC (1:2,000, Invitrogen) with several rinses in between. For double immunostaining of DARPP-32 and VGluT1, Alexa660-conjugated goat anti-mouse and Alexa488-conjugated goat anti-guinea pig antibody were used. For double immunostaining of DARPP-32 and Mef2C, Alexa555-conjugated goat anti-mouse and biotin-conjugated donkey anti-goat antibody were used followed by tyramide-FITC amplification as described above. For double Golgi staining and GFP immunostaining, after Golgi staining, the brain sections were processed for GFP immunostaining using the ABC method with DAB substrate.

### TUNEL staining

Terminal deoxynucleotidyl transferase dUTP nick end labeling (TUNEL) staining to identify apoptotic cells was performed using *In Situ* Cell Death Detection Kit, POD (#11684817910, Roche) with instructions from the manufacturer.

### Western blotting

Western blotting was performed as previously described<sup>45</sup>. Brain tissue lysates containing denatured proteins were resolved by 7.5% Tricine-SDS-PAGE and wet-transferred with transfer buffer (25 mM Tris, 192 mM Glycine and 20% Methanol in distilled H<sub>2</sub>O) to polyvinyl difluoride (PVDF) membranes (Hybond-P, Amersham Biosciences) for 90 min. The protein-bound membranes were blocked with 5% nonfat dry milk in Tris-buffered saline with Tween-20 (TBST; 150 mM NaCl, 25 mM Tris and 0.05% Tween-20, pH 7.4) at room temperature for 1 hr with agitation, and then were incubated with appropriately diluted primary antibody. The dilutions of the primary antibodies were as follows: goat anti-Mef2C (1:1,000; #sc-13266, Santa Cruz), mouse anti-PSD95 (1:4,000; #7E3-1B8, Affinity BioReagents), guinea pig anti-VGluT1 (1:50,000; #ab5905, Millipore), rabbit anti-GluR1 (1:2,000; #ab1504, Millipore), mouse anti- $\beta$ -actin (1:10,000; #A5441, Sigma), and mouse anti-alpha-tubulin (1:10,000; #T9026, Sigma). The primary antibodies were diluted in TBST containing 1% nonfat dry milk at 4°C overnight with gentle shaking. After being washed with TBST for three times, the membranes were incubated with appropriate horseradish peroxidase (HRP)-conjugated secondary antibody (goat anti-mouse or goat anti-guinea pig,



site-directed mutagenesis (Neogene Biomedicals Taiwan/Genscript). The sequences of the AAAT & CAAATT motifs were mutated to GGGT & CGGGTT (MT2) to generate a Mef2C–MT2–c-fos-Luc plasmid. For construction of the human *MEF2C* reporter gene plasmid, the nucleotides of the 5' flanking region of human *MEF2C* gene (–872 to 261 bp, transcription initiation site: +1) were cloned by PCR into the KpnI and NheI sites of pGL3–c-fos-Luc plasmid using genomic DNA of SH-SY5Y cell.

### Reporter gene assay

Mouse Mef2C–pGL3–c-fos-Luc or pGL3–c-fos-Luc plasmids were co-transfected along with pCAG-EYFP–CAG–mFoxp2, pCAG-EYFP–CAG–hFOXP2 or pCAG-EYFP–CAG–hFOXP2<sup>R553H</sup> and pGL4–Renilla plasmids into N2A cells. For the mutant reporter gene assay, Mef2C–MT1–c-fos-Luc or Mef2C–MT2–c-fos-Luc plasmids were co-transfected along with pCAG-EYFP–CAG–mFoxp2, pCAG-EYFP–CAG–hFOXP2 or pCAG-EYFP–CAG–hFOXP2<sup>R553H</sup> and pGL4–Renilla plasmids into N2A cells. For the human MEF2C reporter gene assay, human MEF2C–pGL3–c-fos-Luc or pGL3–c-fos-Luc plasmids were co-transfected along with pCAG-EYFP–CAG–hFOXP2 or pCAG-EYFP–CAG–hFOXP2<sup>R553H</sup> and pGL4–Renilla plasmids into SH-SY5Y cells.

### Chromatin immunoprecipitation

Cultured striatal cells were fixed and processed for chromatin immunoprecipitation assay using the ChIP-IT<sup>®</sup> Express Chromatin Immunoprecipitation Kit (Active Motif) according to the manufacturer's instruction. An affinity-purified polyclonal rabbit anti-Foxp2 antibody (H. Takahashi) was used to immunoprecipitate DNA that was then used as templates for PCR to detect the 5' flanking region of mouse *Mef2C* gene (–1718 to –2131 bp, translational initiation site +1) using forward (5'-TGTCTTAGTGTGTGTTGTTTCATAT-3') and reverse (5'-TAAGCGCTTAGGCAGGCATAGTCC-3') primers. The PCR product size was 414 bp. For ChIP-qPCR, the DNA products of ChIP assays were analyzed by quantitative PCR (Applied Biosystems StepOne system). Briefly, the PCR reaction solution containing 200-fold diluted DNAs and 2X TaqMan<sup>®</sup> Fast Universal PCR Master Mix (Applied Biosystems<sup>®</sup>) and specific primer pair (Mef2C promoter F: 5'-AGGCAGGCATAGTCCGGTAA-3', R: 5'-CATCTCCCTTCCTTTCTCTTAGCT-3'). Each qRT-PCR reaction was performed in triplicate with the following conditions: 95°C for 10 min followed by 40 cycles at 95°C for 10 s, and 60°C for 1 min. The ChIP-qPCR signals from Foxp2 antibody and RNA Pol II antibody reactions were normalized with that of IgG control.

### Electrophysiology

Brains of male P14 *Foxp2<sup>H/H</sup>* and *Foxp2<sup>+/+</sup>* mice were placed into ice-cold sucrose-based cutting solution (85 mM sucrose, 60 mM NaCl, 3.5 mM KCl, 6 mM MgCl<sub>2</sub>, 0.5 mM CaCl<sub>2</sub>, 38 mM NaHCO<sub>3</sub>, 1.25 mM NaH<sub>2</sub>PO<sub>4</sub>, 10 mM HEPES, and 25 mM glucose), and coronal slices (250 μm) were cut (Vibroslice 7000smz, Campden Instruments, UK), incubated in artificial cerebrospinal fluid (aCSF; 120 mM NaCl, 3.5 mM KCl, 1 mM MgCl<sub>2</sub>, 2 mM CaCl<sub>2</sub>, 30 mM NaHCO<sub>3</sub>, 1.25 mM NaH<sub>2</sub>PO<sub>4</sub>, and 15 mM glucose) supplemented with 5 mM HEPES, 1 mM MgCl<sub>2</sub> for 30 min at 35°C, and allowed to recover at room temperature for at least 40 min. Whole-cell patch clamp recordings of SPNs were performed in the

dorsolateral striatum (*Foxp2<sup>H/H</sup>*;  $n = 27$  cells from 6 mice; *Foxp2<sup>+/+</sup>*;  $n = 23$  cells from 4 mice) to measure mEPSCs. SPNs were identified by their size, morphology and characteristic electrophysiological properties including negative resting membrane potentials ( $< -80$  mV), slow capacitance transients and low input resistances<sup>46</sup>. The mean resting membrane potentials were  $-87.5 \pm 0.46$  mV in wildtype mice and  $-84.7 \pm 0.67$  mV in *Foxp2<sup>H/H</sup>* mice; the input resistances were  $176.8 \pm 14.6$  M $\Omega$  in wildtype mice and  $211.0 \pm 13.8$  M $\Omega$  in *Foxp2<sup>H/H</sup>* mice; the cell capacitance levels were  $47.7 \pm 2.2$  pF in wildtype mice and  $44.8 \pm 2.9$  pF in *Foxp2<sup>H/H</sup>* mice; and series resistances during recordings were  $21.5 \pm 1$  M $\Omega$  in wild-type mice and  $18.7 \pm 0.7$  M $\Omega$  in *Foxp2<sup>H/H</sup>* mice. Glass electrodes (5–8 M $\Omega$ ) were filled with an internal solution containing K gluconate (150 mM), NaCl (10 mM), Mg-ATP (4 mM), GTP (0.5 mM), HEPES (10 mM) and EGTA (0.05 mM) adjusted to pH = 7.3 and 310 mOsm. The liquid junction potential (15 mV) was corrected online and the cells were clamped to a membrane potential of  $-85$  mV. Slices were perfused (2–3 ml/min, aCSF, 21–23°C) in the presence the GABA<sub>A</sub> receptor antagonist, SR-95531 (10  $\mu$ M, Sigma), and tetrodotoxin (TTX, 0.1  $\mu$ M, Tocris). All solutions were continuously bubbled with carbogen (95% O<sub>2</sub> and 5% CO<sub>2</sub>). Signals were low-pass filtered at 2.5 kHz and sampled at 20 kHz (EPC-10 amplifier, HEKA, Lambrecht, Germany) using Patchmaster (HEKA). Traces were analyzed with Mini Analysis software (V 6.0.7, Synaptosoft). For electrophysiological recordings in *Foxp2<sup>+/+</sup>* and *Foxp2<sup>-/-</sup>* mice at P8, and in *Nestin-Cre;Mef2C<sup>+/+</sup>* and *Nestin-Cre;Mef2C<sup>fl/fl</sup>* mice at P14, the brains were placed in ice-cold aCSF (119 mM NaCl, 2.5 mM KCl, 26.2 mM NaHCO<sub>3</sub>, 1 mM NaH<sub>2</sub>PO<sub>4</sub>·H<sub>2</sub>O, 1.3 mM MgSO<sub>4</sub>, 11 mM glucose, and 2.5 CaCl<sub>2</sub>) oxygenated with 95% O<sub>2</sub> and 5% CO<sub>2</sub>, and were then cut in the coronal plane at 300  $\mu$ m with a vibrotome. After recovering for 2 hr at 25°C, the brain slices were perfused with oxygenated aCSF containing picrotoxin (100  $\mu$ M, Tocris Bioscience) and tetrodotoxin (1  $\mu$ M, Tocris Bioscience). Whole-cell patch clamp recordings of SPNs were performed in the striatum (*Foxp2<sup>+/+</sup>*;  $n = 8$  cells from 4 mice; *Foxp2<sup>-/-</sup>*;  $n = 7$  cells from 3 mice; *Nestin-Cre;Mef2C<sup>+/+</sup>*;  $n = 7$  cells from 3 mice; and *Nestin-Cre;Mef2C<sup>fl/fl</sup>*;  $n = 9$  cells from 3 mice) with glass pipettes filled with internal solution (131 mM potassium gluconate, 10 mM HEPES, 2 mM EGTA, 20 mM KCl, 8 mM NaCl, 2 mM MgATP, 0.3 mM Na<sub>3</sub>GTP, pH7.2, 300–310 mOsm). Membrane potentials were held at  $-70$  mV by voltage clamp. mEPSCs were recorded with Axon MultiClamp 700B (AutoMate Scientific, USA) for ~10 min. The recorded currents were analyzed with MiniAnalysis (Synaptosoft, USA). The investigator who performed electrophysiological recordings of *Foxp2* knockout and *Mef2C* knockout mice was blind to the genotype of the mice.

## USV analysis

The USV recordings were performed with mouse genotypes blinded to the experimenter. USVs were recorded in pups on P8 during the daylight period of light/dark cycle. After a 30-min habituation period in a soundproof room, each pup was removed from the cage containing its mother and littermates, and was placed in a glass beaker (diameter: 6 cm) in a sound-attenuating plastic chamber. Within the beaker, a microphone (condenser ultrasound microphone Avisoft-Bioacoustics CM16) was hung 6 cm above the pup. After ~1 min of habituation, recordings began and were continued for 5 min (Avisoft UltraSoundGate 116, Avisoft-RECORDER software). The recorded data were transferred to Avisoft-SASLab Pro (Version 5.2) to analyze spectrograms of vocalizations with settings of 50% overlapping



FlatTop windows, 100% frame size and 256 points fast Fourier transform (FFT) length. After de-noising, the automatic single threshold was set to 2 dB above the baseline. The post-filter was set to a maximal entropy of 100. Emitted events with frequency between 40–100 kHz were included, and the following measures were recorded and averaged for each group: events (number of calls), elements (discontinuous signals separated by more than 5-ms duration within a single event); peak frequency at start (the peak frequency at the beginning of each event); peak frequency at end (the peak frequency at the end point of each event); peak amplitude at start (the peak amplitude at the beginning of each event); peak amplitude at end (the peak amplitude at the end point of each event); peak frequency at max (the peak frequency at the point of the maximum amplitude of the entire event); peak amplitude at max (the peak amplitude of the entire event); and frequency jump (abrupt upward increase in frequency exceeding 25 kHz within a single event).

### Quantification of dendritic spine density

Dendritic spines were counted in Golgi-stained material with the aid of light microscopy using a 100X oil immersion objective (Nikon Eclipse E800M; Olympus BX63). Coronal sections of three pairs of brains were used for analysis. For brains of each *Foxp2* genotype, we counted 10 neurons in the dorsomedial striatum and 10 in the dorsolateral striatum. For each *Nestin-Cre;Mef2C* genotype, we counted 13–19 neurons in the dorsomedial striatum and 15–22 neurons in the dorsolateral striatum. For each *Dlx5/6-Cre;Foxp2;Mef2C* genotype, we counted 10–12 neurons in the dorsomedial striatum and 11–17 neurons in the dorsolateral striatum. The number of spines in the proximal parts of secondary dendrites was counted for each neuron. Spine densities were quantified by tracing dendritic segments in which spines were counted. The data were presented as averaged spine number/10  $\mu\text{m}$ . The dendritic spines were categorized into six types (stubby, thin/filopodia, mushroom, branched, multiple-branched and atypical) according to Harris et al.<sup>28</sup> with slight modifications. Thin spine and filopodia were included in the same group as spine/filopodia, because it was difficult to distinguish them with light microscopy. Atypical spines were those that could not be assigned to a specific group. Spines were categorized as ‘stubby’ if the diameter of the neck was similar to the total length of the spine. Spines were categorized as ‘thin/filopodia’ if the length was longer than the neck diameter, and the diameters of the head and neck were similar or the head-neck ratio was less than two. Spines were categorized as ‘mushroom’ if the diameter of the head was at least 2.5 fold the diameter of the neck. Spines were categorized as ‘branched’ spines if they had two heads and as ‘multiple-branched’ if they had more than two heads. For photomicrographic illustration of dendritic spines (Fig. 3d–f and Supplementary Fig. 4a–c), the images were processed with the AutoQuant de-convolution software (Media Cybernetics) to de-blur the images caused by spines oriented in different depths of focal planes.

### Microscopic image analyses

Photomicrographs were acquired using Olympus BX51, BX63 fluorescence microscopes and a Zeiss LSM700 confocal microscope. Quantification of cell number was performed with the aid of Image J software. For comparison between the brains with different genotypes, we analyzed photomicrographs at matched anatomical levels. Fluorescence intensity was measured for single cells (Fig. 2g) or in the region of interest (Figs. 2d,e, 4c,

Fig. 6g–i and Supplementary Fig. 2) using the RGB measure plugins of ImageJ. For quantification of striatal compartmentation (Supplementary Fig. 3a–h), the sum of MOR1-positive striosome areas or CalDAG-GEFI-poor matrix areas was normalized with the total striatal area. For quantification of Foxp2- or Mef2C-positive cells (Fig. 2h and Supplementary Fig. 3), Foxp2- or Mef2C-positive cells were counted in six 0.05-mm<sup>2</sup> squares that were placed evenly in the striatum of each section, and the cell numbers averaged over 3 sections, from rostral to caudal striatal levels, were analyzed with statistical tests described below.

## Statistics

No statistical methods were used to pre-determine sample sizes, but our sample sizes are similar to those generally employed in the field. For small number of samples, we assumed normal distribution because the number of samples was too small for normality tests. Statistical analyses for the data of cell counts, dendritic spine counts, and biochemical and immunochemical measurements of protein levels were done with *Student's* two-tailed *t*-test or analysis of variance (ANOVA) followed by Tukey's post hoc test. Statistical analysis for electrophysiological data was done with Origin (V 8.6, OriginLab; Northampton, USA), by Mann-Whitney *U* test and *Student's* two-tailed *t*-test. Statistical analysis for the USV data was performed with SPSS (IBM, version 21). The USV data were first assessed by the Kolmogorov-Smirnov test for normal distribution exploration. Normally distributed data were processed with one-way ANOVA followed by Tukey's test for post hoc comparisons between two groups. For the data sets without normal distributions, the data were analyzed with Kruskal-Wallis one-way ANOVA followed by Dunn's pairwise multiple comparisons test between two groups. All statistical data were presented as mean ± s.e.m. A supplementary methods checklist is available.

## Data collection and analysis

Animals/samples were assigned to various experimental groups according to their genotypes. Data collection and analysis were not performed blind to the conditions of the experiments, unless specifically specified. No data points were excluded from analyses for any reason.

## Data availability

The data that support the findings of this study are available from the corresponding authors upon request.

## Supplementary Material

Refer to Web version on PubMed Central for supplementary material.

## Acknowledgments

We thank P. Arrollta of Harvard University, K. Campbell of Cincinnati Children's Hospital Medical Center, H.C. Hemmings of Rockefeller University, O. Marin of King's College London and E. Olson of University of Texas Southwestern Medical Center for providing transgenic mice and reagents, M. Bear, M. Sur, M.-M. Poo and D. Homma for insightful discussion, and Y. Kubota for help with illustrations and manuscript preparation. This work was supported by NIH/NICHD grant R37 HD028341 (A.M.G.), the Nancy Lurie Marks Family Foundation

(A.M.G.), the Simons Center for the Social Brain at MIT (A.M.G.), the Paul G. Allen Family Foundation (S.P.), National Science Council grants NSC97-2321-B-010-006, NSC98-2321-B-010-002, NSC99-2321-B-010-002, NSC100-2321-B-010-002, NSC101-2321-B-010-021, NSC102-2321-B-010-018, NSC102-2911-I-010-506 (F.-C.L.), Ministry of Science and Technology grant MOST103-2321-B-010-009, MOST104-2321-B-010-022 (F.-C.L.), National Health Research Institutes grant NHRI-EX104-10429NI, NHRI-EX105-10429NI (F.-C.L.) and by an Aiming for Top University grant, Ministry of Education, Taiwan (F.-C.L.).

## REFERENCES

1. Abrahams BS, Geschwind DH. Advances in autism genetics: on the threshold of a new neurobiology. *Nat. Rev. Genet.* 2008; 9:341–355. [PubMed: 18414403]
2. Mody M, Belliveau JW. Speech and language impairments in autism: insights from behavior and neuroimaging. *N. Am. J. Med. Sci. (Boston)*. 2013; 5:157–161. [PubMed: 24349628]
3. Hollander E, et al. Striatal volume on magnetic resonance imaging and repetitive behaviors in autism. *Biol. Psychiatry*. 2005; 58:226–232. [PubMed: 15939406]
4. Di Martino A, et al. Aberrant striatal functional connectivity in children with autism. *Biol. Psychiatry*. 2011; 69:847–856. [PubMed: 21195388]
5. Watkins KE, et al. MRI analysis of an inherited speech and language disorder: structural brain abnormalities. *Brain*. 2002; 125:465–478. [PubMed: 11872605]
6. Vargha-Khadem F, et al. Neural basis of an inherited speech and language disorder. *Proc. Natl. Acad. Sci. U. S. A.* 1998; 95:12695–12700. [PubMed: 9770548]
7. Groszer M, et al. Impaired synaptic plasticity and motor learning in mice with a point mutation implicated in human speech deficits. *Curr. Biol.* 2008; 18:354–362. [PubMed: 18328704]
8. Enard W, et al. A humanized version of Foxp2 affects cortico-basal ganglia circuits in mice. *Cell*. 2009; 137:961–971. [PubMed: 19490899]
9. Graham SA, Fisher SE. Decoding the genetics of speech and language. *Curr. Opin. Neurobiol.* 2013; 23:43–51. [PubMed: 23228431]
10. Mukamel Z, et al. Regulation of MET by FOXP2, genes implicated in higher cognitive dysfunction and autism risk. *J. Neurosci.* 2011; 31:11437–11442. [PubMed: 21832174]
11. Vernes SC, et al. A functional genetic link between distinct developmental language disorders. *New Engl. J. Med.* 2008; 359:2337–2345. [PubMed: 18987363]
12. Roll P, et al. Molecular networks implicated in speech-related disorders: FOXP2 regulates the SRPX2/uPAR complex. *Hum. Mol. Genet.* 2010; 19:4848–4860. [PubMed: 20858596]
13. Zoghbi HY, Bear MF. Synaptic dysfunction in neurodevelopmental disorders associated with autism and intellectual disabilities. *Cold Spring Harb. Perspect. Biol.* 2012; 4:a009886. [PubMed: 22258914]
14. Ebert DH, Greenberg ME. Activity-dependent neuronal signalling and autism spectrum disorder. *Nature*. 2013; 493:327–337. [PubMed: 23325215]
15. Novara F, et al. Refining the phenotype associated with MEF2C haploinsufficiency. *Clin. Genet.* 2010; 78:471–477. [PubMed: 20412115]
16. Rauch, A.; Bartholdi, D.; Rueegger, CM.; Zweier, M.; Zweier, C.; Bijlsma, EK.; van Haeringen, A.; Reardon, W.; Zollino, M.; Baumer, A. MEF2C mutations are a frequent cause of Rett- or Angelman syndrome like neurodevelopmental disorders; Montreal, Canada. Presented at the 12th International Congress of Human Genetics/61st Annual Meeting of The American Society of Human Genetics; 2011 October 12. Program Number: 1026T
17. Neale BM, et al. Patterns and rates of exonic de novo mutations in autism spectrum disorders. *Nature*. 2012; 485:242–245. [PubMed: 22495311]
18. Spiteri E, et al. Identification of the transcriptional targets of FOXP2, a gene linked to speech and language, in developing human brain. *Am. J. Hum. Genet.* 2007; 81:1144–1157. [PubMed: 17999357]
19. Le Meur N, et al. MEF2C haploinsufficiency caused by either microdeletion of the 5q14.3 region or mutation is responsible for severe mental retardation with stereotypic movements, epilepsy and/or cerebral malformations. *J. Med. Genet.* 2010; 47:22–29. [PubMed: 19592390]

20. Flavell SW, et al. Activity-dependent regulation of MEF2 transcription factors suppresses excitatory synapse number. *Science*. 2006; 311:1008–1012. [PubMed: 16484497]
21. Barbosa AC, et al. MEF2C, a transcription factor that facilitates learning and memory by negative regulation of synapse numbers and function. *Proc. Natl. Acad. Sci. U. S. A.* 2008; 105:9391–9396. [PubMed: 18599438]
22. Tsai NP, et al. Multiple autism-linked genes mediate synapse elimination via proteasomal degradation of a synaptic scaffold PSD-95. *Cell*. 2012; 151:1581–1594. [PubMed: 23260144]
23. Tian X, Kai L, Hockberger PE, Wokosin DL, Surmeier DJ. MEF-2 regulates activity-dependent spine loss in striatopallidal medium spiny neurons. *Mol. Cell Neurosci*. 2010; 44:94–108. [PubMed: 20197093]
24. Nisenbaum LK, Webster SM, Chang SL, McQueeney KD, LoTurco JJ. Early patterning of prelimbic cortical axons to the striatal patch compartment in the neonatal mouse. *Dev. Neurosci*. 1998; 20:113–124. [PubMed: 9691187]
25. Somogyi P, Bolam JP, Smith AD. Monosynaptic cortical input local axon collaterals of identified striatonigral neurons A light and electron microscopic study using the golgi-peroxidase transport degeneration procedure. *J. Comp. Neurol*. 1981; 195:567–584. [PubMed: 6161949]
26. Sheth AN, McKee ML, Bhide PG. The sequence of formation and development of corticostriate connections in mice. *Dev. Neurosci*. 1998; 20:98–112. [PubMed: 9691186]
27. Fremeau RT Jr, Voglmaier S, Seal RP, Edwards RH. VGLUTs define subsets of excitatory neurons and suggest novel roles for glutamate. *Trends Neurosci*. 2004; 27:98–103. [PubMed: 15102489]
28. Harris KM, Jensen FE, Tsao B. Three-dimensional structure of dendritic spines and synapses in rat hippocampus (CA1) at postnatal day 15 and adult ages: implications for the maturation of synaptic physiology and long-term potentiation. *J. Neurosci*. 1992; 12:2685–2705. [PubMed: 1613552]
29. Li S, Weidenfeld J, Morrisey EE. Transcriptional and DNA binding activity of the Foxp1/2/4 family is modulated by heterotypic and homotypic protein interactions. *Mol. Cell Biol*. 2004; 24:809–822. [PubMed: 14701752]
30. Shu W, et al. Altered ultrasonic vocalization in mice with a disruption in the Foxp2 gene. *Proc. Natl. Acad. Sci. U. S. A.* 2005; 102:9643–9648. [PubMed: 15983371]
31. Li H, et al. Transcription factor MEF2C influences neural stem/progenitor cell differentiation and maturation in vivo. *Proc. Natl. Acad. Sci. U. S. A.* 2008; 105:9397–9402. [PubMed: 18599437]
32. Pulipparacharuvil S, et al. Cocaine regulates MEF2 to control synaptic and behavioral plasticity. *Neuron*. 2008; 59:621–633. [PubMed: 18760698]
33. Akhtar MW, et al. vivo analysis of MEF2 transcription factors in synapse regulation and neuronal survival. *PLoS ONE*. 2012; 7:e34863. [PubMed: 22496871]
34. Adachi M, Lin PY, Pranav H, Monteggia LM. Postnatal Loss of Mef2c Results in Dissociation of Effects on Synapse Number and Learning and Memory. *Biol. Psychiatry*. 2015 Article in Press.
35. Sia GM, Clem RL, Haganir RL. The human language-associated gene SRPX2 regulates synapse formation and vocalization in mice. *Science*. 2013; 342:987–991. [PubMed: 24179158]
36. Schulz SB, Haesler S, Scharff C, Rochefort C. Knockdown of FoxP2 alters spine density in Area X of the zebra finch. *Genes Brain Behav*. 2010; 9:732–740. [PubMed: 20528955]
37. Haesler S, et al. Incomplete and inaccurate vocal imitation after knockdown of FoxP2 in songbird basal ganglia nucleus Area X. *PLoS Biol*. 2007; 5:e321. [PubMed: 18052609]
38. Chahrour M, et al. MeCP2, a key contributor to neurological disease, activates and represses transcription. *Science*. 2008; 320:1224–1229. [PubMed: 18511691]
39. Morrow EM, et al. Identifying autism loci and genes by tracing recent shared ancestry. *Science*. 2008; 321:218–223. [PubMed: 18621663]
40. Crittenden JR, Graybiel AM. Basal Ganglia disorders associated with imbalances in the striatal striosome and matrix compartments. *Front. Neuroanat*. 2011; 5:59. [PubMed: 21941467]
41. Lipton SA, et al. Autistic phenotype from MEF2C knockout cells. *Science*. 2009; 323:208.

## ADDITIONAL REFERENCES FOR ONLINE METHODS

42. Tronche F, et al. Disruption of the glucocorticoid receptor gene in the nervous system results in reduced anxiety. *Nat. Genet.* 1999; 23:99–103. [PubMed: 10471508]
43. Stenman J, Toresson H, Campbell K. Identification of two distinct progenitor populations in the lateral ganglionic eminence: implications for striatal and olfactory bulb neurogenesis. *J. Neurosci.* 2003; 23:167–174. [PubMed: 12514213]
44. Lu KM, Evans SM, Hirano S, Liu FC. Dual role for Islet-1 in promoting striatonigral and repressing striatopallidal genetic programs to specify striatonigral cell identity. *Proc. Natl. Acad. Sci. U. S. A.* 2014; 111:E168–E177. [PubMed: 24351932]
45. Chang SL, et al. Ectopic expression of nolz-1 in neural progenitors promotes cell cycle exit/premature neuronal differentiation accompanying with abnormal apoptosis in the developing mouse telencephalon. *PLoS ONE.* 2013; 8:e74975. [PubMed: 24073229]
46. Pawlak V, Kerr JN. Dopamine receptor activation is required for corticostriatal spike-timing-dependent plasticity. *J. Neurosci.* 2008; 28:2435–2446. [PubMed: 18322089]

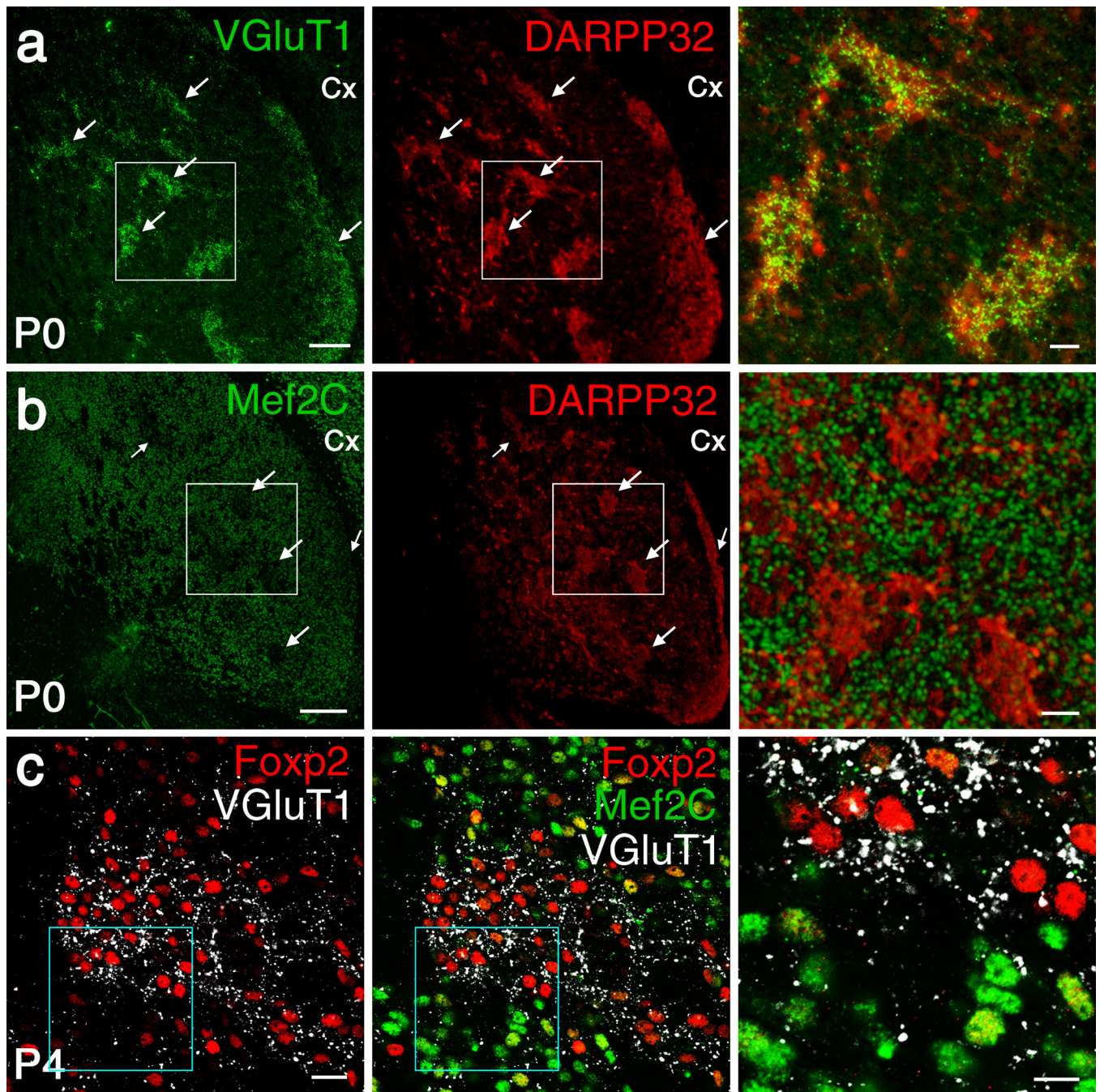


**Figure 1.** Dissociation of Foxp2 and Mef2C in SPNs is initiated in VGlut1-positive (VGlut1<sup>+</sup>) striosomes in neonatal striatum. (a,b) Dual-antibody immunostaining shows VGlut1<sup>+</sup> corticostriatal axon terminals in P0 striatum (a, left, arrows) clustered in DARPP-32<sup>+</sup> striosomes (a, middle, arrows) that are devoid of Mef2C (b, arrows). Boxed regions in a and b are shown as merged images at higher magnification in the right panels of a and b. (c) In P4 striatum, VGlut1-rich, Mef2C-poor striosomes contain clustered, strongly Foxp2<sup>+</sup> cells.

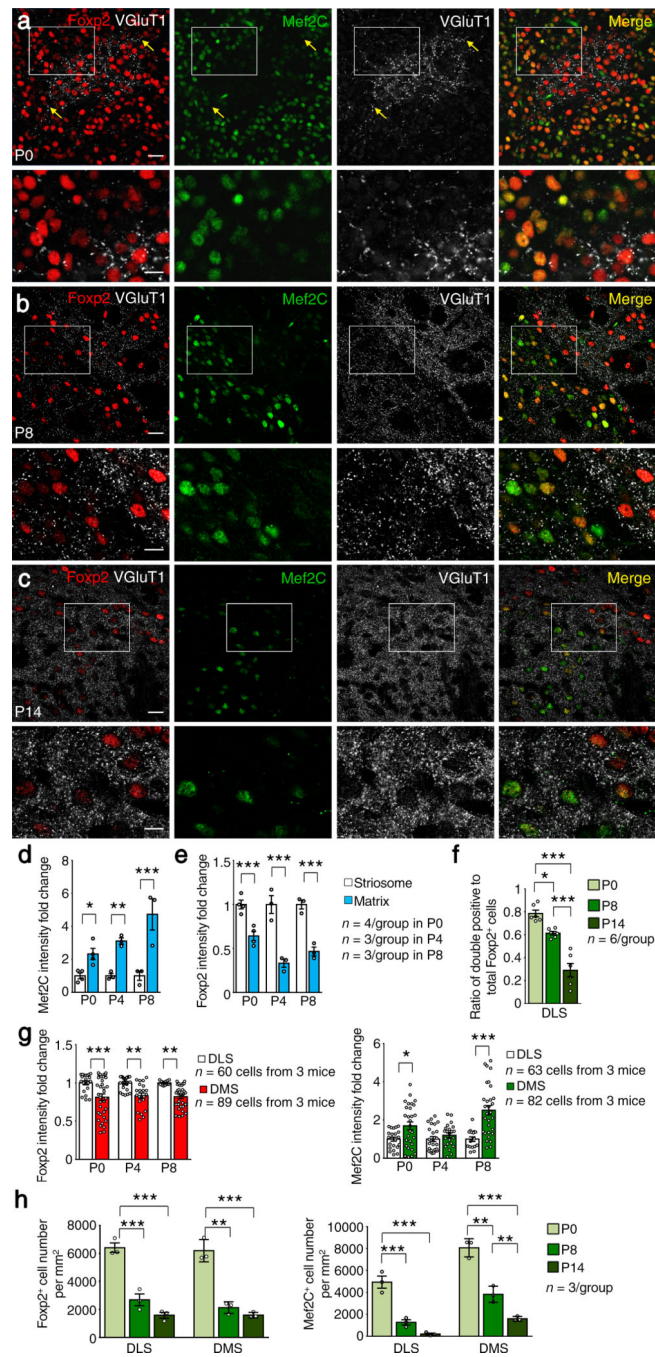
Images represent five repeats. Scale bars: 100  $\mu\text{m}$  (in **a, b, left and middle**), 25  $\mu\text{m}$  (in **a, b, right**), 20  $\mu\text{m}$  (in **c, left and middle**) and 10  $\mu\text{m}$  (in **c, right**).

Author Manuscript

Author Manuscript

Author Manuscript

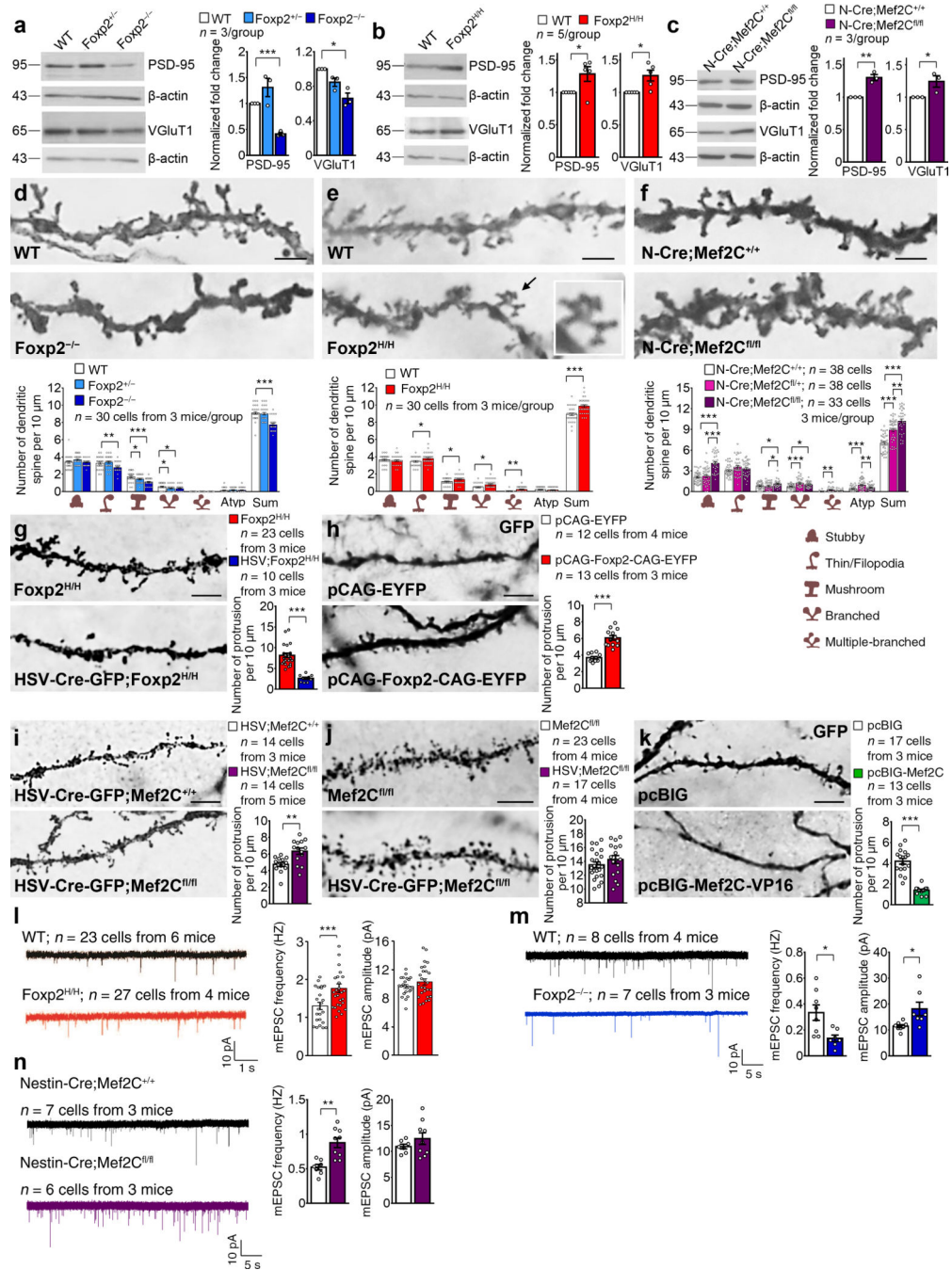
Author Manuscript



**Figure 2.** Progressive dissociation of Foxp2 and Mef2C in SPNs during postnatal development. (a–c) Triple-antibody immunostaining shows predominant concentration of VGluT1<sup>+</sup> corticostriatal axonal puncta in striosomes that are Mef2C–poor but exhibit strong Foxp2 immunostaining in P0 (a) and P8 (b) striatum. By P14 (c), VGluT1<sup>+</sup> corticostriatal axonal puncta become widespread and relatively evenly distributed in the striatum, and Foxp2 expression is equally widespread, whereas Mef2C is down-regulated. The boxed regions in a–c are shown at high magnification at bottom rows. Note that strongly Foxp2<sup>+</sup> cells express

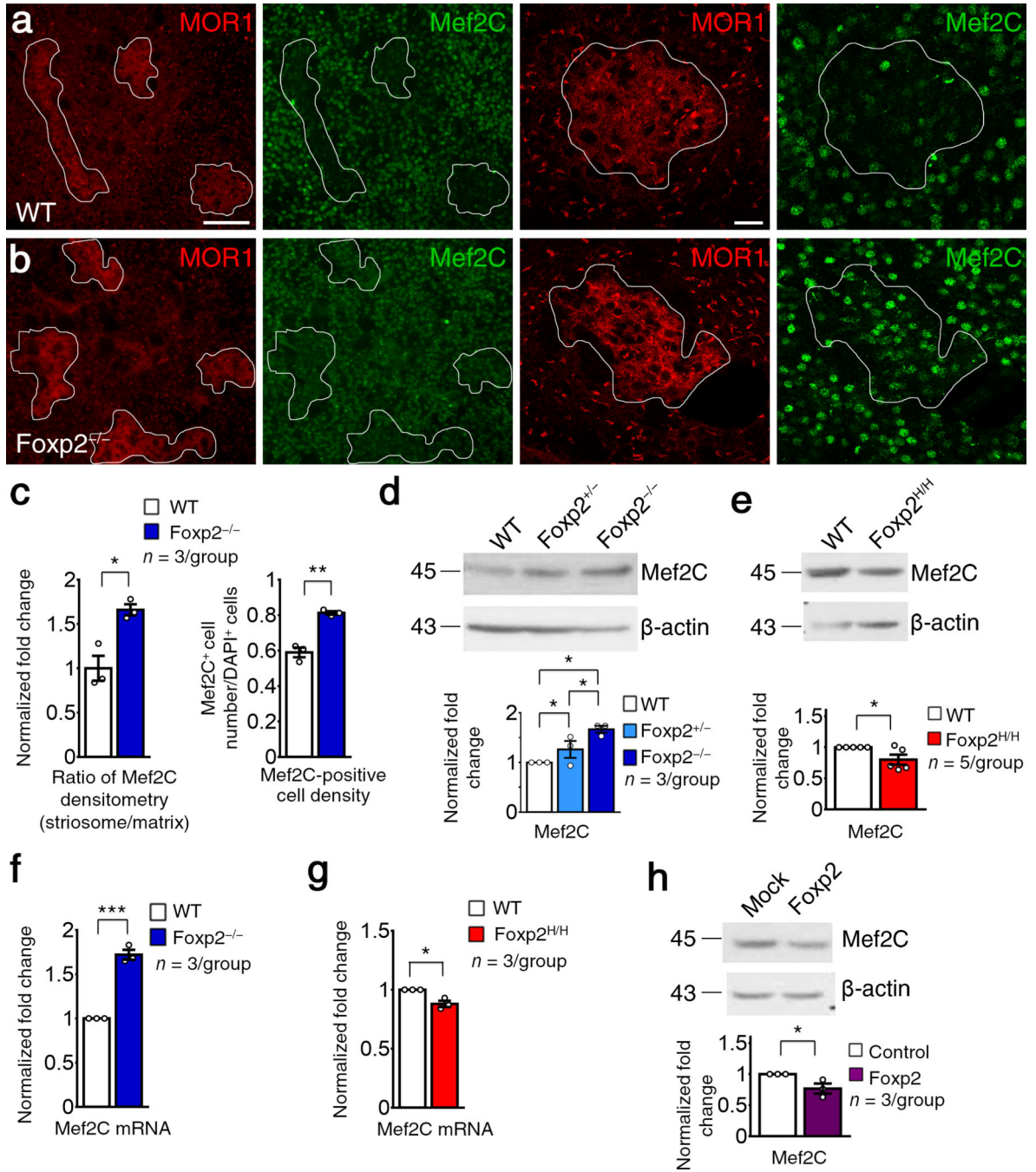


weak Mef2C, and vice versa. Yellow arrows in **a** mark the boundary of a striosome. Scale bars: 20  $\mu\text{m}$  (top rows) and 10  $\mu\text{m}$  (bottom rows). Images represent five repeats. (**d,e**) Mef2C (**d**) and Foxp2 (**e**) immunofluorescence intensity in P0-P8 wildtype striatum. Data represent at least three mice per group. (**f**) Ratio of cells positive for both Foxp2 and Mef2C relative to total Foxp2<sup>+</sup> cells in the dorsolateral striatum ( $n = 6$  mice/group). (**g**) Ratio of Foxp2 (left) or Mef2C (right) immunofluorescence intensity in striosomes of dorsomedial striatum (DMS) relative to that in dorsolateral striatum (DLS). Data represent at least 60 cells from three mice per group. (**h**) The densities of Foxp2<sup>+</sup> and Mef2C<sup>+</sup> cells in DLS and DMS of wildtype mice ( $n = 3$  mice/group). \* $P < 0.05$ , \*\* $P < 0.01$ , \*\*\* $P < 0.001$ . Error bars represent s.e.m. Two-way ANOVA with Tukey's honest significant difference (HSD) post hoc test are used in **d**,  $F_{(2, 16)} = 4.400$ ,  $P = 0.033$  for interaction,  $F_{(1, 16)} = 49.072$ ,  $P = 0.000006$  for compartment,  $F_{(2, 16)} = 4.400$ ,  $P = 0.033$  for age, in **e**,  $F_{(2, 16)} = 3.456$ ,  $P = 0.060$  for interaction,  $F_{(1, 16)} = 110.852$ ,  $P = 0.000000$  for compartment,  $F_{(2, 16)} = 3.001$ ,  $P = 0.060$  for age, and in **g**, for Foxp2,  $F_{(2, 139)} = 0.039$ ,  $P = 0.962$  for interaction,  $F_{(1, 139)} = 40.321$ ,  $P = 0.000000$  for region,  $F_{(2, 139)} = 0.039$ ,  $P = 0.962$  for age; for Mef2C,  $F_{(2, 141)} = 5.838$ ,  $P = 0.004$  for interaction,  $F_{(1, 141)} = 25.477$ ,  $P = 0.000001$  for region.  $F_{(2, 141)} = 5.838$ ,  $P < 0.004$  for age. One-way ANOVA with Tukey's HSD post hoc test is used in **f**,  $F_{(2, 15)} = 41.852$ ,  $P = 0.000001$ , and in **h**, for Foxp2,  $F_{(2, 6)} = 56.571$ ,  $P = 0.000128$  in DLS,  $F_{(2, 6)} = 67.197$ ,  $P = 0.000078$  in DMS; for Mef2C,  $F_{(2, 6)} = 50.443$ ,  $P = 0.000177$  in DLS,  $F_{(2, 6)} = 75.536$ ,  $P = 0.000056$  in DMS.



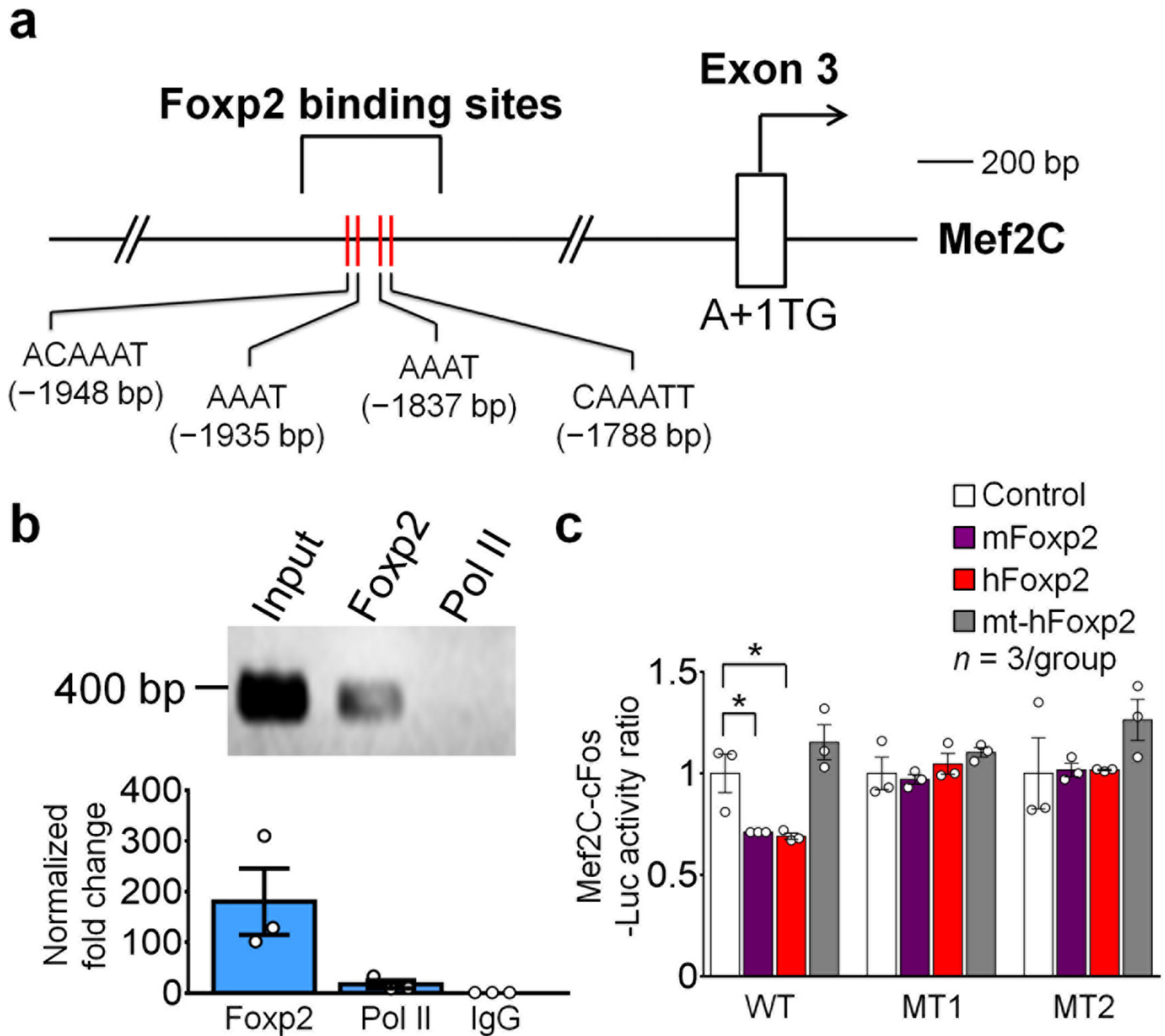
**Figure 3.** Synaptic proteins and dendritic spines of SPNs are oppositely regulated by *Foxp2* and *Mef2C*. (a–c) Western blots showing expression of PSD-95 and VGluT1 proteins in the P12 *Foxp2*<sup>-/-</sup> striatum (a), P14 *Foxp2*<sup>H/H</sup> striatum (b) and P14 *Mef2C* knockout striatum (c). Data represent at least three mice per genotype. Full-length blots are presented in Supplementary Fig. 10. (d–f) Golgi staining showing dendritic spines in dorsolateral SPNs of *Foxp2*<sup>-/-</sup> mice (d), *Foxp2*<sup>H/H</sup> (e) and *Mef2C* knockout (f) mice. Inset in e: multiple-branched spines. Data represent at least 30 cells from three mice per genotype. Atyp:

atypical. Scale bars: 2.5  $\mu\text{m}$ . **(g)** Intrastratial injection of HSV-Cre-GFP virus in P2 *Foxp2<sup>H/H</sup>* mice decreases spine density in GFP-positive SPNs at P8. **(h)** *In utero* electroporation of pCAG-EYFP-CAG-Foxp2 at E13.5 increases spines of P14 wildtype SPNs. Scale bar: 5  $\mu\text{m}$ . **(i,j)** Intrastratial injection of HSV-Cre-GFP virus in *Mef2C<sup>f/f</sup>* mice at P2 increases spines in GFP-positive SPNs at P8 **(i)**, but the same injection at P14-P15 does not affect spine counts at P19-P20 **(j)**. Scale bars: 5  $\mu\text{m}$ . **(k)** *In utero* electroporation of pcBIG-Mef2C-VP16 at E12.5 decreases spines of P14 wildtype SPNs. Scale bar: 5  $\mu\text{m}$ . Data in **g–k** represent at least 10 cells from three mice per group. **(l–n)** mEPSC recordings of SPNs in *Foxp2<sup>H/H</sup>* **(l)**, *Foxp2<sup>-/-</sup>* **(m)**, and *Mef2C* knockout **(n)** mice. Data represent at least 7 cells from at least three mice per genotype. \* $P < 0.05$ , \*\* $P < 0.01$ , \*\*\* $P < 0.001$ . Error bars represent s.e.m. One-way ANOVA with Tukey's HSD post hoc test are used in **a**, for VGluT1,  $F_{(2, 6)} = 14.649$ ,  $P = 0.005$ ; for PSD-95,  $F_{(2, 6)} = 19.954$ ,  $P = 0.002$ , **d''**, for stubby,  $F_{(2, 87)} = 2.992$ ,  $P = 0.055$ ; for thin/filopodia,  $F_{(2, 87)} = 8.396$ ,  $P = 0.000463$ ; for mushroom,  $F_{(2, 87)} = 12.889$ ,  $P = 0.000013$ ; for branched,  $F_{(2, 87)} = 4.169$ ,  $P = 0.019$ ; for atypical,  $F_{(2, 87)} = 0.293$ ,  $P = 0.747$ ; for sum,  $F_{(2, 87)} = 28.470$ ,  $P = 0.000000$ , **f''**, for stubby,  $F_{(2, 106)} = 34.658$ ,  $P = 0.000000$ ; for thin/filopodia,  $F_{(2, 106)} = 2.012$ ,  $P = 0.139$ ; for mushroom,  $F_{(2, 106)} = 5.182$ ,  $P = 0.007$ ; for branched,  $F_{(2, 106)} = 9.555$ ,  $P = 0.000153$ ; for multiple branched,  $F_{(2, 106)} = 5.965$ ,  $P = 0.004$  for atypical,  $F_{(2, 106)} = 11.944$ ,  $P = 0.000021$ ; for sum,  $F_{(2, 106)} = 38.448$ ,  $P = 0.000000$ . Student's *t* test are used in **b**, for VGluT1,  $t_{(8)} = -3.155$ ,  $P = 0.014$ ; for PSD-95,  $t_{(8)} = 2.518$ ,  $P = 0.036$ , **c**, for PSD-95,  $t_{(4)} = -6.442$ ,  $P = 0.003$ ; for VGluT1,  $t_{(4)} = -2.795$ ,  $P = 0.049$ , **e''**, for stubby,  $t_{(29)} = 0.623$ ,  $P = 0.538$ ; for thin/filopodia,  $t_{(29)} = -2.249$ ,  $P = 0.032$ ; for mushroom,  $t_{(29)} = -2.041$ ,  $P = 0.050$ ; for branched,  $t_{(29)} = -2.300$ ,  $P = 0.029$ ; for multiple branched,  $t_{(29)} = -3.525$ ,  $P = 0.001$ , for atypical,  $t_{(29)} = 0.769$ ,  $P = 0.448$ ; for sum,  $t_{(29)} = -4.216$ ,  $P = 0.000383$ , **g**,  $t_{(31)} = 9.429$ ,  $P = 0.000000$ , **h**,  $t_{(23)} = -7.612$ ,  $P = 0.000001$ , **i**,  $t_{(26)} = -3.509$ ,  $P = 0.002$ , **j**,  $t_{(38)} = -1.122$ ,  $P = 0.269$ , **k**,  $t_{(28)} = 9.453$ ,  $P = 0.000000$ , **l**, for frequency,  $t_{(13)} = 2.890$ ,  $P = 0.013$ ; for amplitude,  $t_{(13)} = -2.2505$ ,  $P = 0.043$ , and **n**, for frequency,  $t_{(14)} = -4.022$ ,  $P = 0.001$ , for amplitude,  $t_{(14)} = -1.131$ ,  $P = 0.237$ . Mann-Whitney U test are used in **m**,  $U = 167.5$ ,  $P = 0.009$  for frequency and  $U = 273$ ,  $P = 0.471$  for amplitude.

**Figure 4.**

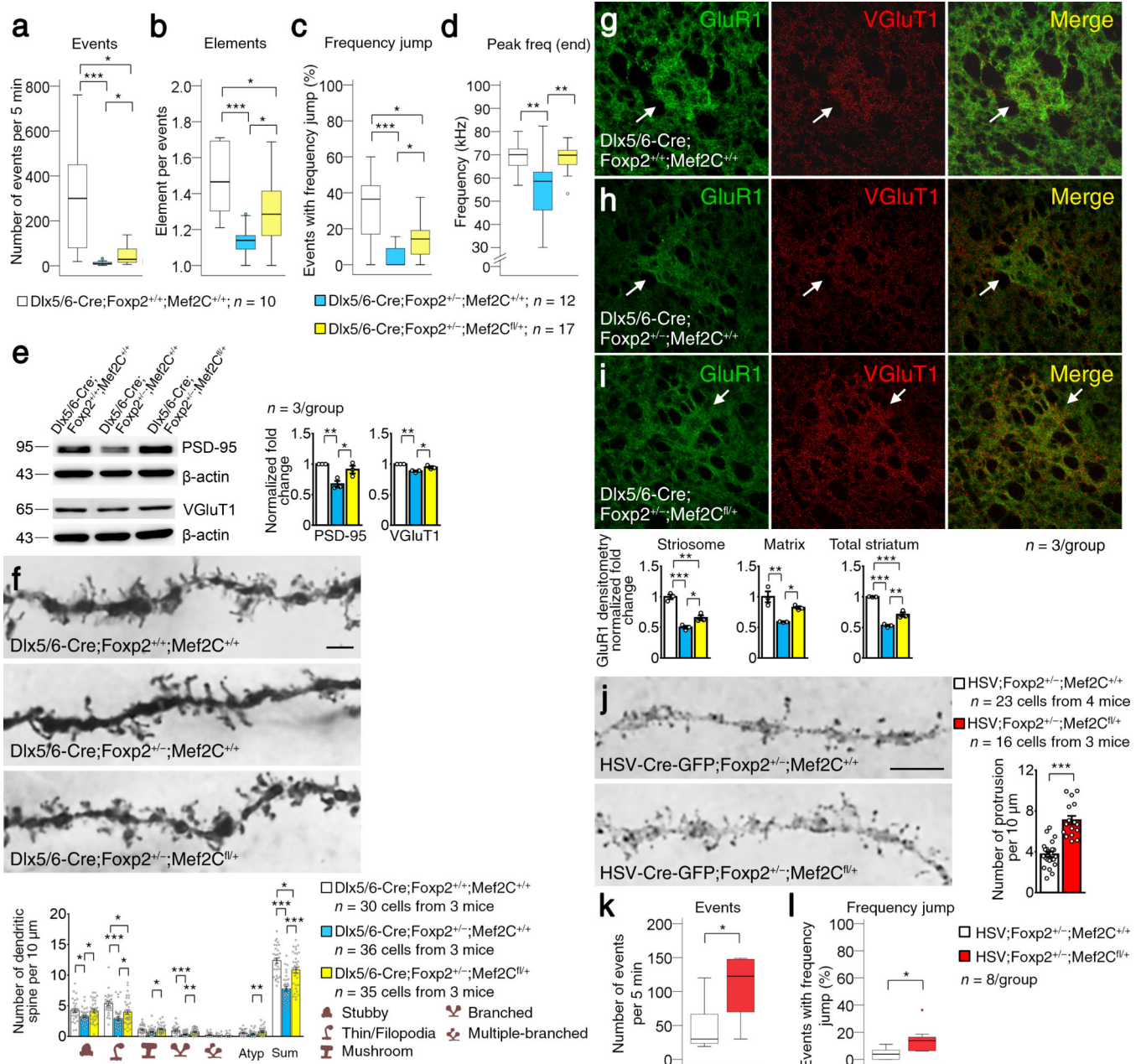
*Foxp2* suppresses *Mef2C* expression in SPNs. (a–b) Dual immunostaining of *Mef2C* and MOR1 in P7 wildtype (a) and *Foxp2*<sup>-/-</sup> (b) striatum. Scale bars: 50  $\mu\text{m}$  (a, two left panels) and 20  $\mu\text{m}$  (a, two right panels). (c) Ratio of immunofluorescence intensity of *Mef2C*<sup>+</sup> SPNs in striosomes over those in the matrix in *Foxp2*<sup>-/-</sup> mice compared to wildtype mice (left, Student's *t* test;  $t_{(4)} = -4.317$ ,  $P = 0.012$ ), and density of *Mef2C*-positive cells in P7 *Foxp2*<sup>-/-</sup> striatum relative to wildtype (right,  $t_{(4)} = -7.692$ ,  $P = 0.002$ ). Images and data represent three mice per group. (d,e) Western blots showing expression of *Mef2C* protein in

P12 *Foxp2*<sup>-/-</sup> striatum (**d**; *Foxp2*<sup>+/+</sup> vs. *Foxp2*<sup>+/-</sup>:  $P = 0.022$ ,  $t_{(4)} = -3.645$ ; *Foxp2*<sup>+/-</sup> vs. *Foxp2*<sup>-/-</sup>:  $P = 0.018$ ,  $t_{(4)} = -3.875$ ; *Foxp2*<sup>+/+</sup> vs. *Foxp2*<sup>-/-</sup>:  $P = 0.016$ ,  $t_{(4)} = -7.913$ ) and P14 *Foxp2*<sup>H/H</sup> striatum (**e**;  $t_{(8)} = 2.480$ ,  $P = 0.038$ ). Data represent at least three mice per genotype. (**f,g**) qRT-PCR analyses of *Mef2C* mRNA levels in P12 *Foxp2*<sup>-/-</sup> striatum (**f**;  $t_{(4)} = -12.987$ ,  $P < 0.001$ ) and P14 *Foxp2*<sup>H/H</sup> striatum (**g**;  $t_{(4)} = 4.540$ ,  $P = 0.010$ ). Data represent three mice per genotype. (**h**) Western blots showing the level of Mef2C protein in N2A cells transfected with *Foxp2* expressing plasmid ( $t_{(4)} = 2.853$ ,  $P = 0.046$ ). Data represent three repeats. Full-length blots are presented in Supplementary Fig. 10. \* $P < 0.05$ , \*\* $P < 0.01$ . Error bars represent s.e.m.



**Figure 5.**

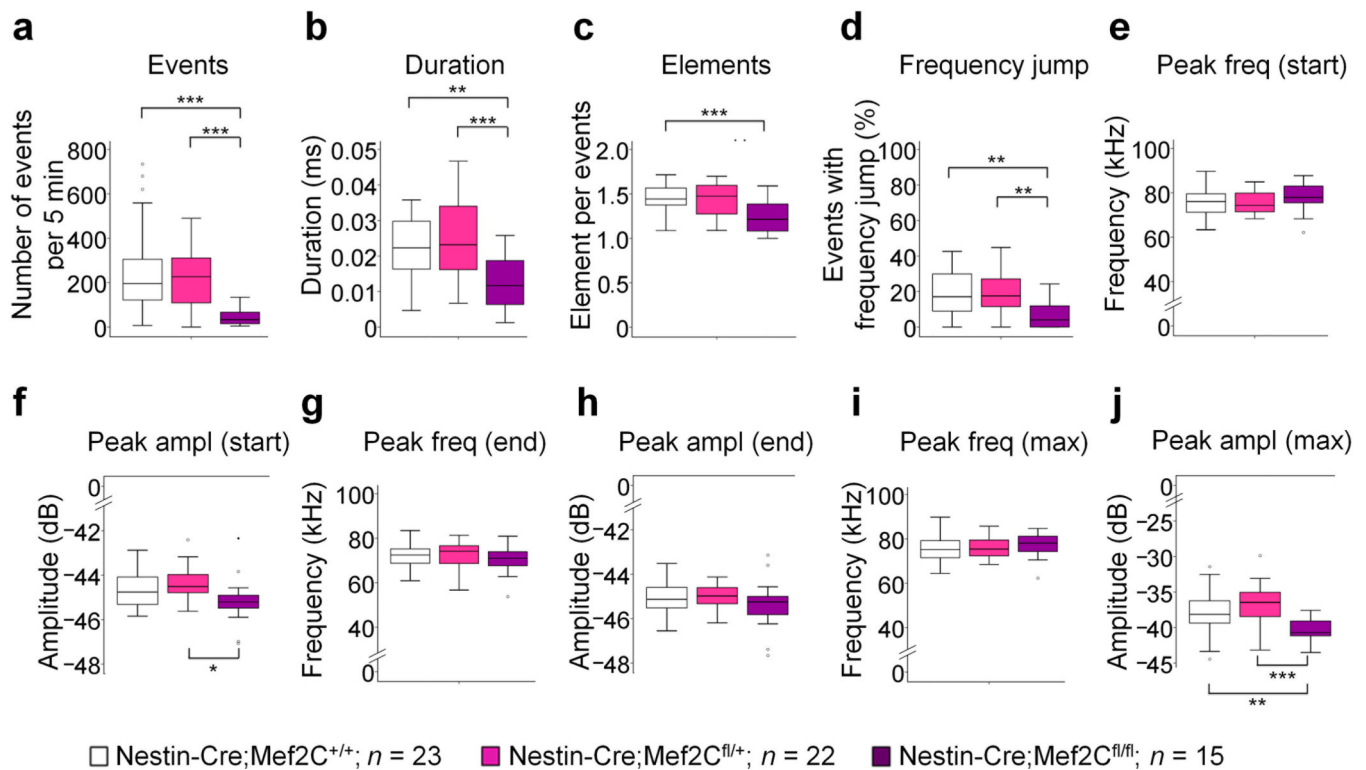
*Mef2C* is a direct target gene of *Foxp2*. (a) Foxp2 binding motifs in the second intron of mouse *Mef2C* gene. (b) ChIP-qPCR analysis of E16 striatum. Foxp2 antibody, but not the control Pol II antibody, immunoprecipitates a DNA fragment containing the two pairs of Foxp2 motifs. Full-length gel is presented in Supplementary Fig. 10. (c) Transfection of mouse *Foxp2* or human *FOXP2* plasmids, but not transfection of human *FOXP2*<sup>R553H</sup> mutant (mt-hFOXP2) plasmid, represses luciferase activity of Mef2C–pCL3–c-fos-Luc reporter in N2A cells. Repression by mouse *Foxp2* or human *FOXP2* in wildtypes (WT) is abolished with Mef2C–MT1–c-fos-Luc (MT1) or Mef2C–MT2–c-fos-Luc (MT2) mutant plasmids (Student's *t* test; WT: control vs. mFoxp2,  $t_{(4)} = 3.017$ ,  $P = 0.039$ ; control vs. hFoxp2,  $t_{(4)} = 3.237$ ,  $P = 0.032$ ). Data represent three repeats. \* $P < 0.05$ . Error bars represent s.e.m.

**Figure 6.**

Inactivation of one allele of *Mef2C* rescues USV, dendritic spines and synaptic protein changes in P8 *Foxp2*<sup>+/-</sup> mice. (**a-d**) Analysis of USVs in P8 *Dlx5/6-Cre;Foxp2*<sup>+/-</sup>;*Mef2C*<sup>+/+</sup> (white), *Dlx5/6-Cre;Foxp2*<sup>+/-</sup>;*Mef2C*<sup>+/+</sup> (blue) and *Dlx5/6-Cre;Foxp2*<sup>+/-</sup>;*Mef2C*<sup>fl/+</sup> (yellow) mice. Box plots show the median (horizontal line in the box), range between the 25<sup>th</sup> and 75<sup>th</sup> percentiles (box), and 1.5 times this interquartile range (T-bars). Circles show outlying values. Data represent at least ten mice per genotype. (**e**) Western blots showing increased expression of PSD-95 and VGluT1 protein expression in P8 *Dlx5/6-Cre;Foxp2*<sup>+/-</sup>;*Mef2C*<sup>+/+</sup>; *Dlx5/6-Cre;Foxp2*<sup>+/-</sup>;*Mef2C*<sup>+/+</sup> and *Dlx5/6-Cre;Foxp2*<sup>+/-</sup>;*Mef2C*<sup>fl/+</sup> striatum. Data represent three mice per genotype. Full-length blots

are presented in Supplementary Fig. 10. **(f)** SPN dendritic spines of P8 *Dlx5/6-Cre;Foxp2<sup>+/+</sup>;Mef2C<sup>+/+</sup>* (top), *Dlx5/6-Cre;Foxp2<sup>+/-</sup>;Mef2C<sup>+/+</sup>* (middle) and *Dlx5/6-Cre;Foxp2<sup>+/-</sup>;Mef2C<sup>fl/+</sup>* (bottom) mice. Data represent at least 30 cells from three mice per genotype. Scale bars: 2.5  $\mu\text{m}$ . **(g–i)** GluR1 immunofluorescence in striosomes and matrix of P8 *Dlx5/6-Cre;Foxp2<sup>+/+</sup>;Mef2C<sup>+/+</sup>* **(g)**, *Dlx5/6-Cre;Foxp2<sup>+/-</sup>;Mef2C<sup>+/+</sup>* **(h)** and *Dlx5/6-Cre;Foxp2<sup>+/-</sup>;Mef2C<sup>fl/+</sup>* **(i)** striatum. Images and data represent three mice per genotype. Scale bars: 50  $\mu\text{m}$ . **(j)** Dendritic spines are increased in SPNs of HSV-*Cre;Foxp2<sup>+/-</sup>;Mef2C<sup>fl/+</sup>* mice (red) compared to that in control SPNs of HSV-*Cre;Foxp2<sup>+/-</sup>;Mef2C<sup>+/+</sup>* mice (white). Data represent at least 16 cells from three mice per group. Scale bars: 5  $\mu\text{m}$ . **(k,l)** The events **(k)** and frequency jump **(l)** are increased in HSV-*Cre-GFP;Foxp2<sup>+/-</sup>;Mef2C<sup>fl/+</sup>* mice compared to control HSV-*Cre-GFP;Foxp2<sup>+/-</sup>;Mef2C<sup>+/+</sup>* mice. Data represent 8 mice per group. \* $P < 0.05$ , \*\* $P < 0.01$ , \*\*\* $P < 0.001$ . Error bars represent s.e.m. Kruskal-Wallis one-way ANOVA followed by Dunn's pairwise multiple comparisons test are used in **a**, test statistic = 21.474,  $P < 0.001$ , **c**, test statistic = 15.832,  $P < 0.001$ . One way ANOVA are used in **b**,  $F_{(2, 36)} = 10.768$ ,  $P = 0.000238$ , **d**,  $F_{(2, 36)} = 7.296$ ,  $P = 0.002$ , **e**, for PSD-95,  $F_{(2, 6)} = 12.645$ ,  $P = 0.007$ ; for VGluT1,  $F_{(2, 6)} = 21.487$ ,  $P = 0.002$ , **f**, for stubby,  $F_{(2, 98)} = 4.521$ ,  $P = 0.013$ ; for thin/filopodia,  $F_{(2, 98)} = 13.875$ ,  $P = 0.000005$ ; for mushroom,  $F_{(2, 98)} = 3.816$ ,  $P = 0.025$ ; for branched,  $F_{(2, 98)} = 11.563$ ,  $P = 0.000031$ ; for multiple branched,  $F_{(2, 98)} = 2.023$ ,  $P = 0.138$ , for atypical,  $F_{(2, 98)} = 4.709$ ,  $P = 0.011$ ; for sum,  $F_{(2, 98)} = 30.941$ ,  $P = 0.000000$ , **g–i**, for striosome,  $F_{(2, 6)} = 54.063$ ,  $P = 0.000145$ ; for matrix,  $F_{(2, 6)} = 15.055$ ,  $P = 0.005$ ; for total striatum,  $F_{(2, 6)} = 117.718$ ,  $P = 0.000015$ . *Student's t* test is used in **j**,  $t_{(26)} = -7.410$ ,  $P = 0.000000$ , **k**,  $t_{(14)} = -2.789$ ,  $P = 0.014$ , and **l**,  $t_{(14)} = -2.727$ ,  $P = 0.016$ .



**Figure 7.**

Reduction of USVs in *Nestin-Cre;Mef2C* knockout mice at P8. The number of USV calls (**a**; one-way ANOVA with Tukey's HSD post hoc test;  $F_{(2, 66)} = 11.001$ ,  $P = 0.000196$ ), call durations (**b**;  $F_{(2, 66)} = 8.613$ ,  $P = 0.000475$ ), numbers of elements in each call (**c**;  $F_{(2, 66)} = 6.444$ ,  $P = 0.003$ ), proportion of events with frequency jumps (**d**;  $F_{(2, 66)} = 5.723$ ,  $P = 0.005$ ) and maximum peak amplitudes (**j**;  $F_{(2, 66)} = 10.022$ ,  $P = 0.000371$ ) are decreased in *Nestin-Cre;Mef2C<sup>fl/fl</sup>* mice, compared to those in control *Nestin-Cre;Mef2C<sup>+/+</sup>* mice, whereas peak frequency at start (**e**;  $F_{(2, 66)} = 2.497$ ,  $P = 0.090$ ) and end (**g**;  $F_{(2, 66)} = 0.069$ ,  $P = 0.933$ ) of calls, amplitudes at start (**f**;  $F_{(2, 66)} = 4.404$ ,  $P = 0.016$ ) and end (**h**;  $F_{(2, 66)} = 1.325$ ,  $P = 0.273$ ) of calls, and maximum peak frequency (**i**;  $F_{(2, 66)} = 1.218$ ,  $P = 0.303$ ) are not affected. Data represent at least 15 mice per genotype. Box plots show the median (horizontal line in the box), range between the 25<sup>th</sup> and 75<sup>th</sup> percentiles (box), and 1.5 times this interquartile range (T-bars). Outlying values are marked as circles. \* $P < 0.05$ , \*\* $P < 0.01$ , \*\*\* $P < 0.001$ .